Monte Carlo simulation of ultrafast processes in photoexcited semiconductors: Coherent and incoherent dynamics

Monte Carlo simulation of ultrafast processes in photoexcited semiconductors: Coherent and incoherent dynamics

Tilmann Kuhn* and Fausto Rossi
Dipartimento di Fisica, Università di Modena, Via Campi 213/A, 41100 Modena, Italy
(Received 25 February 1992)

The ultrafast dynamics of photoexcited carriers in a semiconductor is investigated by using a Monte Carlo simulation. In addition to a "conventional" Monte Carlo simulation, the coherence of the external light field and the resulting coherence in the carrier system are fully taken into account. This allows us to treat the correct time dependence of the generation process showing a time-dependent linewidth associated with a recombination from states off resonance due to stimulated emission. The subsequent dephasing of the carriers due to scattering processes is analyzed. In addition, the simulation contains the carrier-carrier interaction in Hartree-Fock approximation giving rise to a band-gap renormalization and excitonic effects which cannot be treated in a conventional Monte Carlo simulation where polarization effects are neglected. Thus the approach presents a unified numerical method for the investigation of phenomena occurring close to the band gap and those typical for the energy relaxation of hot carriers.

I. INTRODUCTION

The technological progress in the generation of ultrashort laser pulses, together with the possibility of detecting processes on this time scale, has led to a series of experiments that gave new insight into the microscopic carrier dynamics in a semiconductor. A phenomenon that has been widely investigated in recent years is the energy relaxation of photoexcited carriers.[1-10] This process typically occurs on a picosecond or femtosecond time scale. Different experimental techniques have been used: luminescence experiments—either band to band,[1-7] where the product of the distribution functions in the valence and conduction bands are monitored, or band to acceptor,[8,9] which is sensitive only to the electron distribution—as well as pump-and-probe experiments,[10] which yield information on the sum of the distribution functions. In addition, theoretical analysis has been performed using different techniques: analytical or numerical solutions of model equations starting from parametrized distribution functions,[11-13] a direct integration of the Boltzmann equation,[14-17] and Monte Carlo simulations.[7,18-26] Most quantitative investigations have used the latter method because it seems best suited to include on a microscopic level a variety of scattering processes (carrier-phonon, carrier-carrier, carrier plasmon, inter-valence-band, intervalley, etc). The role of these scattering processes, in turn, is influenced by the choice of experimental conditions: carrier-carrier scattering and hot-phonon effects strongly depend on the density, and intervalley transitions are suppressed if the excitation is below the threshold for this process. Thus, the combination of experimental results and theoretical calculations give detailed information on the relevant scattering rates and coupling constants.

However, there is another class of experiments that have attracted much interest in the last years and which cannot be included simply in these simulations. These are experiments investigating coherent phenomena like the dephasing of an electron-hole plasma[27] or of excitons,[28-35] or the dynamical Stark effect.[36,37] The reason is that for these phenomena the distribution functions, which are the basic quantities for semiclassical transport theory and which are calculated within a Monte Carlo simulation, do not provide sufficient information to describe the physical situation. In addition, information concerning the interband polarization is needed. This polarization is created due to the coherence of the external light field interacting with the semiconductor, as well as to the Coulomb interaction between electrons and holes. This latter effect is of particular importance in energy regions close to the band gap. For the theoretical analysis of coherent phenomena, a fully quantum-mechanical treatment is required. Various methods have been used in the literature: Bogoliubov transformation,[38,39] band-edge equations,[40-42] Green's-function techniques,[43-47] and density-matrix theory.[42,48-52] Due to the increased difficulty in obtaining numerical solutions when compared with the semiclassical case, however, the incoherent-scattering mechanisms here are often treated either in relaxation time approximation, or only few interaction mechanisms are taken into account.

In particular, on short time scales the two classes of phenomena cannot be separated. The light of an ultrashort laser pulse in general has a strong degree of coherence and therefore introduces coherence in the carrier system. If the physical phenomena under investigation occur on a time scale shorter than the dephasing time, i.e., the time after which coherence effects are damped out, they should be taken into account in a theoretical analysis even if the measured quantities, e.g., energy relaxation rates, are variables which are purely determined by distribution functions.

The aim of this work is to present a method which retains the advantages of the Monte Carlo method in treating scattering processes and at the same time to generalize it in order to take into account coherent effects. This requires in addition to a simulation of the distribution functions of the various carrier types, as is done in the semiclassical case, a calculation of the polarizations in-

troduced by the coherent light field. The use of the polarizations as dynamic variables then enables us to take into account also intraband and interband effects of the carrier-carrier interaction which lead in Hartree-Fock approximation to an internal field and a renormalization of the energies. Furthermore, the generation process is treated in a self-consistent way, where the broadening due to the finite pulse duration does not have to be introduced as a phenomenological parameter, but comes out automatically with its full time dependence. At the beginning of the pulse, the linewidth is much larger than at later times due to energy-time uncertainty. Since the narrowing with increasing time is related to a stimulated recombination from the states off resonance, this process has to be included in the simulation. In a "particle picture," as is used typically in a Monte Carlo simulation, this creates some problems, which will be resolved by using an "occupation number picture." This representation also eliminates the conceptual problem in the semiclassical modelization where carriers are treated as distinguishable particles and thus more information than possible is known. It is analogous to the method of cellular automata recently introduced to solve the semiclassical Boltzmann equation for space-dependent problems.[53,54]

The physical model used in the present paper is still strongly simplified with respect to a real semiconductor. In particular, only one valence band and the central valley of the conduction band are taken into account, and the second-order contribution of the carrier-carrier interaction, which would give rise to real scattering processes, is neglected. Therefore, we do not want to compare our results quantitatively with existing experiments. Rather, the aim is to present the method for the simulation and discuss the effects which usually are not taken into account in a Monte Carlo simulation. However, the method described here is open to be extended, e.g., to more bands and other types of interactions. The results will be presented in a future work.

The paper is organized as follows: In Sec. II we present the physical model and derive the relevant equations of motion. In Sec. III the method used for the numerical simulation is presented, emphasizing in particular the differences with respect to a "conventional" ensemble Monte Carlo simulation. Section IV then shows results of the simulations which are divided into the two classes: (a) excitation far from the gap and (b) excitation close to the gap. Finally, in Sec. V we draw some conclusions.

II. THEORETICAL APPROACH

We consider a bulk semiconductor with two parabolic bands, the conduction band and the heavy-hole band. The system is described by a Hamiltonian which, as usual, can be decomposed into a part H_0, which is treated exactly, and a part H_1 describing interactions, which is treated within some approximation scheme. In a semiclassical kinetic picture only the free carriers as well as the various types of free quasiparticles (phonons, photons, etc.) are included in H_0. All interactions between carriers and other types of quasiparticles, and in particular also the interaction of the carriers with the external light field, gives contributions to H_1. They are treated as scattering processes between the different states described by H_0 and the corresponding rates are obtained by using Fermi's golden rule. These approximations lead to the Boltzmann transport equation (BTE) for the distribution functions of the carriers, which is the basis for the theoretical investigation of the carrier kinetics.

On this semiclassical level all coherence or correlation effects are neglected. However, there are two main features where such effects can become important: One is due to the external light field. The light emitted by a laser is at least partially coherent and thus also introduces coherence in the carrier system. This is of particular importance in ultrashort processes since the pulses created, e.g., by mode coupling in the laser resonator, have a high degree of coherence and, on the other hand, scattering processes which destroy the coherence in the carrier system are not yet very effective. The second feature is excitonic effects introduced by the electron-hole interaction. They result in strong electron-hole correlations and largely influence the absorption and emission spectra in a region close to the band gap. As a consequence, the carrier kinetics in this energy range will be different from that obtained from the BTE.

Both phenomena require a treatment that takes not only the distribution functions of electrons and holes as kinetic variables but also the interband polarizations. Then, the interaction with the external light field due to the laser pulse has to be included in H_0, since it is this interaction which creates a coherent polarization. Electron-hole interaction cannot be included in H_0 because it is a two-particle process. However, the explicit knowledge of the polarization enables us to treat it within Hartree-Fock approximation which gives terms linear in the interaction matrix element. Thus, it is one order lower than the carrier-carrier scattering processes in the BTE obtained from Fermi's golden rule.

A. Unperturbed Hamiltonian

The unperturbed Hamiltonian H_0 for the system under investigation is given by

$$H_0 = H_0^c + \sum_i H_0^i \ , \tag{1}$$

where H_0^c is the part of the carriers and the H_0^i are the contributions of the various quasiparticles (phonons, photons, etc.) which are considered for interactions. The carrier part in an electron-hole picture is given by

$$H_0^c = \sum_{\mathbf{k}} \epsilon_{\mathbf{k}}^e c_{\mathbf{k}}^\dagger c_{\mathbf{k}} + \sum_{\mathbf{k}} \epsilon_{\mathbf{k}}^h d_{\mathbf{k}}^\dagger d_{\mathbf{k}} + \sum_{\mathbf{k}} [M_{\mathbf{k}} A^{(+)}(t) c_{\mathbf{k}}^\dagger d_{-\mathbf{k}}^\dagger + M_{\mathbf{k}}^* A^{(-)}(t) d_{-\mathbf{k}} c_{\mathbf{k}}] \ . \tag{2}$$

Here, $c_{\mathbf{k}}^\dagger$ ($c_{\mathbf{k}}$) denote the creation (annihilation) operators of an electron in state $\mathbf{k}$, $d_{\mathbf{k}}^\dagger$ ($d_{\mathbf{k}}$) the corresponding operators for holes, $\epsilon_{\mathbf{k}}^e = E_G + \hbar^2 k^2/2m_e$ and $\epsilon_{\mathbf{k}}^h = \hbar^2 k^2/2m_h$ the energies of electron and hole states, E_G the energy gap, and m_e (m_h) the electron (hole) effective mass. The external light field is treated on a semiclassical level

and within the rotating-wave approximation. $M_{\mathbf{k}}$ is the dipole matrix element and $A^{(+)}$ ($A^{(-)}$) the positive (negative) frequency part of the light field given by

$$A^{(+)}=A_0(t)e^{-i\omega_L t}, \quad A^{(-)}=A^{(+)*} . \tag{3}$$

It is centered at the frequency ω_L, and the pulse shape is given by $A_0(t)$.

The physics of the system can be described within different approaches. One is the method of nonequilibrium Green's functions.[43-47] It has advantages of a formal treatment due to the possibility of a diagrammatic representation, and it is particularly well suited for stationary processes where the Dyson equation can be simplified by means of a Fourier transformation. For time-dependent processes, such as are the subject of this work, the density-matrix method[42,48-52] provides a more transparent approach, since the quantities are more directly related to physical observables. Both methods are strongly related: The density matrix coincides with the equal-time Green's function $G^{<}$ (in the Kadanoff-Baym notation[55] or G^{-+} (in the Keldysh notation[56]). Here, we adopt the density-matrix method.

To describe the kinetics of the system, we first need the distribution functions (intraband density matrices) of electrons and holes, defined as

$$f_{\mathbf{k}}^e=\langle c_{\mathbf{k}}^\dagger c_{\mathbf{k}}\rangle \quad \text{and} \quad f_{\mathbf{k}}^h=\langle d_{\mathbf{k}}^\dagger d_{\mathbf{k}}\rangle . \tag{4}$$

In order to describe the coherence phenomena, we need additionally the two contributions to the interband polarization (interband density matrix), given by

$$p_{\mathbf{k}}=\langle d_{-\mathbf{k}} c_{\mathbf{k}}\rangle \quad \text{and} \quad p_{\mathbf{k}}^*=\langle c_{\mathbf{k}}^\dagger d_{-\mathbf{k}}^\dagger\rangle . \tag{5}$$

Using the Heisenberg equations of motion for the electron and hole operators, we obtain a closed set of equations of motion for the distribution functions and the polarization:

$$\frac{d}{dt}f_{\mathbf{k}}^e=\frac{d}{dt}f_{-\mathbf{k}}^h=g_{\mathbf{k}}^0(t) , \tag{6}$$

$$\frac{d}{dt}p_{\mathbf{k}}=\frac{1}{i\hbar}[(\epsilon_{\mathbf{k}}^e+\epsilon_{-\mathbf{k}}^h)p_{\mathbf{k}} + M_{\mathbf{k}}A_0(t)e^{-i\omega_L t}(1-f_{\mathbf{k}}^e-f_{-\mathbf{k}}^h)] , \tag{7}$$

and the complex-conjugate equation for $p_{\mathbf{k}}^*$. The generation rate $g_{\mathbf{k}}^0$ is given by

$$g_{\mathbf{k}}^0=\frac{1}{i\hbar}[M_{\mathbf{k}}A_0(t)e^{-i\omega_L t}p_{\mathbf{k}}^*-M_{\mathbf{k}}^*A_0^*(t)e^{i\omega_L t}p_{\mathbf{k}}] . \tag{8}$$

The main difference between the generation rate (8) and the results obtained from Fermi's golden rule is the fact that in the present approach, the generation process, when considering only the distribution functions as relevant variables, is retarded, as can be seen by formally integrating Eq. (7) and eliminating the polarization in Eq. (8). The generation rate at time t depends not only on the light field and the distribution functions at time t but also on earlier times. If the amplitude $A_0(t)$ is sufficiently slowly varying, a Markov approximation is possible and the semiclassical result containing the energy-conserving δ function is recovered. For ultrashort pulses, however, this approximation is not valid and the energy-time uncertainty relation leads to a broadening of the generation rate. In a semiclassical treatment, this broadening has to be taken into account in a phenomenological way. In the present treatment it comes out automatically with its full time dependence. In addition, it turns out that the generation rate is not strictly positive definite even if the phase-space filling factor $(1-f_{\mathbf{k}}^e-f_{-\mathbf{k}}^h)$ does not play a role. Thus, a simulation also has to include the process of recombination stimulated by the external field. The consequences for the simulation as well as the results and differences with respect to a semiclassical treatment will be discussed in Secs. III and IV.

Without interactions, Eqs. (6) and (7) describe a set of independent two-level systems driven by an external field with a variable detuning $\delta_{\mathbf{k}}=\epsilon_{\mathbf{k}}^e+\epsilon_{-\mathbf{k}}^h-\hbar\omega_L$ between the transition energy and the light frequency. The dynamics is fully coherent. It is equivalent to a set of atoms in a strong light field, and the equations of motion are the well-known optical Bloch equations in the absence of damping. These equations are modified by the various interaction mechanisms. The common feature of all contributions due to the interaction Hamiltonian is the fact that creation and annihilation operators of the carriers and the corresponding quasiparticles appear at least in third order. Thus, in general we cannot obtain closed equations of motion for a finite set of expectation values as was the case for the distribution functions and the polarizations when considering only H_0. Instead, we obtain a hierarchy of equations which has to be truncated within some approximation scheme.

These interaction mechanisms lead to additional contributions in the equations of motion:

$$\frac{d}{dt}f_{\mathbf{k}}^e=g_{\mathbf{k}}^0(t)+\sum_i \left.\frac{d}{dt}f_{\mathbf{k}}^e\right|^i , \tag{9}$$

$$\frac{d}{dt}f_{\mathbf{k}}^h=g_{-\mathbf{k}}^0(t)+\sum_i \left.\frac{d}{dt}f_{\mathbf{k}}^h\right|^i , \tag{10}$$

$$\frac{d}{dt}p_{\mathbf{k}}=\frac{1}{i\hbar}[(\epsilon_{\mathbf{k}}^e+\epsilon_{-\mathbf{k}}^h)p_{\mathbf{k}} + M_{\mathbf{k}}A_0(t)e^{-i\omega_L t}(1-f_{\mathbf{k}}^e-f_{-\mathbf{k}}^h)] + \sum_i \left.\frac{d}{dt}p_{\mathbf{k}}\right|^i , \tag{11}$$

where the summation is over the various types of interactions. In the following the interaction mechanisms taken into account and the respective approximations performed will be discussed, and the corresponding contributions entering Eqs. (9)–(11) will be derived.

B. Carrier-carrier interaction

The carriers that are created by the laser field are charged particles and thus interact via the Coulomb potential $V_{\mathbf{q}}$. In a two-band model the total interaction (H_1^{cc}) can be separated into three parts: electron-electron interaction (H_1^{ee}), hole-hole interaction (H_1^{hh}), and

electron-hole interaction (H_1^{eh}). They are given, respectively, by

$$H_1^{ee}=\frac{1}{2}\sum_{\mathbf{k},\mathbf{k}',\mathbf{q}} V_{\mathbf{q}} c_{\mathbf{k}+\mathbf{q}}^{\dagger} c_{\mathbf{k}'-\mathbf{q}}^{\dagger} c_{\mathbf{k}'} c_{\mathbf{k}} \ , \tag{12}$$

$$H_1^{hh}=\frac{1}{2}\sum_{\mathbf{k},\mathbf{k}',\mathbf{q}} V_{\mathbf{q}} d_{\mathbf{k}+\mathbf{q}}^{\dagger} d_{\mathbf{k}'-\mathbf{q}}^{\dagger} d_{\mathbf{k}'} d_{\mathbf{k}} \ , \tag{13}$$

$$H_1^{eh}=-\sum_{\mathbf{k},\mathbf{k}',\mathbf{q}} V_{\mathbf{q}} c_{\mathbf{k}+\mathbf{q}}^{\dagger} d_{\mathbf{k}'-\mathbf{q}}^{\dagger} d_{\mathbf{k}'} c_{\mathbf{k}} \ . \tag{14}$$

We have neglected terms that do not conserve the number of each carrier type, i.e., impact ionization and Auger recombination, as well as the interband exchange interaction, which is justified if the excitation binding energy is small compared to the band gap.[43] Using the Heisenberg equations of motion, the resulting carrier-carrier contributions to the equations of motion for the distribution functions and the polarization are given by

$$\left.\frac{d}{dt} f_{\mathbf{k}}^{e}\right|^{cc}=\frac{1}{i\hbar}\sum_{\mathbf{k}',\mathbf{q}} V_{\mathbf{q}}[-\langle c_{\mathbf{k}-\mathbf{q}}^{\dagger} c_{\mathbf{k}'+\mathbf{q}}^{\dagger} c_{\mathbf{k}'} c_{\mathbf{k}}\rangle + \langle c_{\mathbf{k}}^{\dagger} c_{\mathbf{k}'+\mathbf{q}}^{\dagger} c_{\mathbf{k}'} c_{\mathbf{k}+\mathbf{q}}\rangle + \langle c_{\mathbf{k}+\mathbf{q}}^{\dagger} d_{\mathbf{k}'-\mathbf{q}}^{\dagger} d_{\mathbf{k}'} c_{\mathbf{k}}\rangle - \langle c_{\mathbf{k}}^{\dagger} d_{\mathbf{k}'-\mathbf{q}}^{\dagger} d_{\mathbf{k}'} c_{\mathbf{k}-\mathbf{q}}\rangle] \ , \tag{15}$$

$$\left.\frac{d}{dt} f_{\mathbf{k}}^{e}\right|^{cc}=\frac{1}{i\hbar}\sum_{\mathbf{k}',\mathbf{q}} V_{\mathbf{q}}[-\langle d_{\mathbf{k}-\mathbf{q}}^{\dagger} d_{\mathbf{k}'+\mathbf{q}}^{\dagger} c_{\mathbf{k}'} d_{\mathbf{k}}\rangle + \langle d_{\mathbf{k}}^{\dagger} d_{\mathbf{k}'+\mathbf{q}}^{\dagger} d_{\mathbf{k}'} d_{\mathbf{k}+\mathbf{q}}\rangle + \langle c_{\mathbf{k}'+\mathbf{q}}^{\dagger} d_{\mathbf{k}-\mathbf{q}}^{\dagger} d_{\mathbf{k}} c_{\mathbf{k}'}\rangle - \langle c_{\mathbf{k}'+\mathbf{q}}^{\dagger} d_{\mathbf{k}}^{\dagger} d_{\mathbf{k}+\mathbf{q}} c_{\mathbf{k}'}\rangle] \ , \tag{16}$$

$$\left.\frac{d}{dt} p_{\mathbf{k}}\right|^{cc}=\frac{1}{i\hbar}\sum_{\mathbf{k}',\mathbf{q}} V_{\mathbf{q}}[\langle d_{-\mathbf{k}} c_{\mathbf{k}'+\mathbf{q}}^{\dagger} c_{\mathbf{k}'} c_{\mathbf{k}+\mathbf{p}}\rangle + \langle d_{\mathbf{k}'-\mathbf{q}}^{\dagger} d_{\mathbf{k}'} d_{-\mathbf{k}-\mathbf{q}} c_{\mathbf{k}}\rangle - \langle d_{-\mathbf{k}} d_{\mathbf{k}'-\mathbf{q}} d_{\mathbf{k}'} c_{\mathbf{k}-\mathbf{q}}\rangle - \langle c_{\mathbf{k}'+\mathbf{q}}^{\dagger} c_{\mathbf{k}'} d_{-\mathbf{k}+\mathbf{q}} c_{\mathbf{k}}\rangle] \ . \tag{17}$$

The lowest-order approximation is obtained by factorizing the expectation values into distribution functions and polarizations. This constitutes the Hartree-Fock approximation, and the results are

$$\left.\frac{d}{dt} f_{\mathbf{k}}^{e}\right|^{cc}=\frac{1}{i\hbar}\sum_{\mathbf{k}'} V_{\mathbf{k}-\mathbf{k}'}(p_{\mathbf{k}'}^{*} p_{\mathbf{k}}-p_{\mathbf{k}}^{*} p_{\mathbf{k}'}) =\frac{1}{i\hbar}(\Delta_{\mathbf{k}} p_{\mathbf{k}}^{*}-\Delta_{\mathbf{k}}^{*} p_{\mathbf{k}}) \ , \tag{18}$$

$$\left.\frac{d}{dt} f_{-\mathbf{k}}^{h}\right|^{cc}=\frac{1}{i\hbar}\sum_{\mathbf{k}'} V_{\mathbf{k}-\mathbf{k}'}(p_{\mathbf{k}'}^{*} p_{\mathbf{k}}-p_{\mathbf{k}}^{*} p_{\mathbf{k}'}) =\frac{1}{i\hbar}(\Delta_{\mathbf{k}} p_{\mathbf{k}}^{*}-\Delta_{\mathbf{k}}^{*} p_{\mathbf{k}}) \ , \tag{19}$$

$$\left.\frac{d}{dt} p_{\mathbf{k}}\right|^{cc}=-\frac{1}{i\hbar}\sum_{\mathbf{k}'} V_{\mathbf{k}-\mathbf{k}'}[(1-f_{\mathbf{k}}^{e}-f_{-\mathbf{k}}^{h}) p_{\mathbf{k}'} + (f_{\mathbf{k}'}^{e}+f_{-\mathbf{k}'}^{h}) p_{\mathbf{k}}] =\frac{1}{i\hbar}[\Sigma_{\mathbf{k}} p_{\mathbf{k}}+\Delta_{\mathbf{k}}(1-f_{\mathbf{k}}^{e}-f_{-\mathbf{k}}^{h})] \ , \tag{20}$$

where we have introduced the self-energy

$$\Sigma_{\mathbf{k}}=-\sum_{\mathbf{k}'} V_{\mathbf{k}-\mathbf{k}'}(f_{\mathbf{k}'}^{e}+f_{-\mathbf{k}'}^{h}) \tag{21}$$

due to electron-electron and hole-hole interaction, and the internal field

$$\Delta_{\mathbf{k}}=-\sum_{\mathbf{k}'} V_{\mathbf{k}-\mathbf{k}'} p_{\mathbf{k}'} \tag{22}$$

due to electron-hole interaction. Comparing with Eqs. (6)–(8), we see that carrier-carrier interaction in Hartree-Fock approximation leads to a renormalization of the carrier energies by the self-energy $\Sigma_{\mathbf{k}}$ and the renormalization of the external field by an internal field $\Delta_{\mathbf{k}}$. The self-energy is a real quantity; thus there is no incoherent scattering. First-order contributions are still fully coherent. The effect of the internal field on the dynamics of the distribution functions can be included in the generation rate

$$g_{\mathbf{k}}=\frac{1}{i\hbar}\{[M_{\mathbf{k}} A_0(t) e^{-i\omega_L t}+\Delta_{\mathbf{k}}] p_{\mathbf{k}}^{*} - [M_{\mathbf{k}}^{*} A_0^{*}(t) e^{i\omega_L t}+\Delta_{\mathbf{k}}^{*}] p_{\mathbf{k}}\} \ , \tag{23}$$

now calculated with the external and the internal fields. The contribution due to the internal field satisfies the sum rule

$$\sum_{\mathbf{k}} (\Delta_{\mathbf{k}} p_{\mathbf{k}}^{*}-\Delta_{\mathbf{k}}^{*} p_{\mathbf{k}})=0 \ , \tag{24}$$

which demonstrates that it does not really generate carriers. The total number of each carrier type remains constant. Rather, it changes the distribution of carriers inside one band as if it were a scattering process. But, in contrast to a usual scattering process, it is a coherent process which cannot be simply described by a rate equation like the BTE and which does not contribute to a finite lifetime (imaginary part of $\Sigma_{\mathbf{k}}$).

The equations of motion still have the form of optical Bloch equations without damping. Due to the presence of renormalized energies and fields, however, they now are nonlinear equations. These nonlinearities lead to a variety of new phenomena not present in the case of atoms.[43,57]

The presence of free carriers leads to a screening of the bare Coulomb potential. The detailed calculation of the screening is a problem by itself[58] and approximations on various levels can be performed (see, e.g., the discussion in Ref. 47). Here we use the screened Hartree-Fock approximation with a Lindhard-like static screening, where

$$V_{\mathbf{q}}=\frac{e^2}{4\pi\epsilon_0\epsilon_s}\frac{1}{q^2+k_s^2} \ , \tag{25}$$

and the RPA screening wave vector is calculated self-consistently according to[18]

$$k_s^2=\frac{e^2}{\epsilon_0\epsilon_s V}\sum_{\mathbf{k}}-\left[\frac{\partial\epsilon}{\partial k}\right]^{-1}\left[\frac{\partial f_{\mathbf{k}}}{\partial k}\right]. \tag{26}$$

The next step in treating carrier-carrier interaction would be a calculation of the second-order contributions, which introduces incoherent-scattering processes.[47,49] However, in this paper we shall limit ourselves to the first order in carrier-carrier interaction and leave the extension to second order to a future work.

C. Carrier-phonon interaction

Besides the interaction with other carriers, a carrier interacts also with perturbations of the periodicity of the ideal lattice. These interactions can be separated into interactions with static lattice irregularities (impurities, dislocations, alloy disorder, etc.) and those with dynamic degrees of freedom (optical and acoustic phonons). The former ones lead to elastic-scattering processes, which, for the present case of a spatially homogeneous problem without external field, do not contribute to the relaxation process. Thus we have to deal only with carrier-phonon interaction. Introducing the creation (annihilation) operators $b_{\mathbf{q}}^{\dagger}$ ($b_{\mathbf{q}}$) of a phonon with wave vector $\mathbf{q}$, the Hamiltonian describing electron-phonon interaction is given by

$$H_1^{ep}=\sum_{\mathbf{q},\mathbf{k}}(\gamma_{\mathbf{q}}^{e}c_{\mathbf{k}+\mathbf{q}}^{\dagger}b_{\mathbf{q}}c_{\mathbf{k}}+\gamma_{\mathbf{q}}^{e*}c_{\mathbf{k}}^{\dagger}b_{\mathbf{q}}^{\dagger}c_{\mathbf{k}+\mathbf{q}}). \tag{27}$$

Hole-phonon interaction is described by the analogous Hamiltonian

$$H_1^{hp}=\sum_{\mathbf{q},\mathbf{k}}(\gamma_{\mathbf{q}}^{h}d_{\mathbf{k}+\mathbf{q}}^{\dagger}b_{\mathbf{q}}d_{\mathbf{k}}+\gamma_{\mathbf{q}}^{h*}d_{\mathbf{k}}^{\dagger}b_{\mathbf{q}}^{\dagger}d_{\mathbf{k}+\mathbf{q}}), \tag{28}$$

and the contribution of the free phonons to H_0 is given by

$$H_0^{p}=\sum_{\mathbf{q}}\hbar\omega_q b_{\mathbf{q}}^{\dagger}b_{\mathbf{q}}. \tag{29}$$

The structure of the Hamiltonian is independent of the specific type of phonon (acoustic or optical) and of the interaction (polar or deformation potential). The former is specified by the dispersion relation $\omega_{\mathbf{q}}$, and the latter by the interaction matrix element $\gamma_{\mathbf{q}}^{e,h}$. In the numerical analysis discussed in Sec. III, we take into account the interaction with optical phonons via Fröhlich interaction, and with acoustic phonons via deformation-potential coupling. Because the theoretical derivation in this section depends only on the structure of the Hamiltonian, it is the same for both types.

Using the Heisenberg equations of motion, we obtain

$$\left.\frac{d}{dt}f_{\mathbf{k}}^{e}\right|^{cp}=\frac{1}{i\hbar}\sum_{\mathbf{q}}[\gamma_{\mathbf{q}}^{e}(\langle c_{\mathbf{k}}^{\dagger}b_{\mathbf{q}}c_{\mathbf{k}-\mathbf{q}}\rangle-\langle c_{\mathbf{k}+\mathbf{q}}^{\dagger}b_{\mathbf{q}}c_{\mathbf{k}}\rangle)+\gamma_{\mathbf{q}}^{e*}(\langle c_{\mathbf{k}}^{\dagger}b_{\mathbf{q}}^{\dagger}c_{\mathbf{k}+\mathbf{q}}\rangle-\langle c_{\mathbf{k}-\mathbf{q}}^{\dagger}b_{\mathbf{q}}^{\dagger}c_{\mathbf{k}}\rangle)], \tag{30}$$

$$\left.\frac{d}{dt}f_{\mathbf{k}}^{h}\right|^{cp}=\frac{1}{i\hbar}\sum_{\mathbf{q}}[\gamma_{\mathbf{q}}^{h}(\langle d_{\mathbf{k}}^{\dagger}b_{\mathbf{q}}d_{\mathbf{k}-\mathbf{q}}\rangle-\langle d_{\mathbf{k}+\mathbf{q}}^{\dagger}b_{\mathbf{q}}d_{\mathbf{k}}\rangle)+\gamma_{\mathbf{q}}^{h*}(\langle d_{\mathbf{k}}^{\dagger}b_{\mathbf{q}}^{\dagger}d_{\mathbf{k}+\mathbf{q}}\rangle-\langle d_{\mathbf{k}-\mathbf{q}}^{\dagger}b_{\mathbf{q}}^{\dagger}d_{\mathbf{k}}\rangle)], \tag{31}$$

$$\left.\frac{d}{dt}p_{\mathbf{k}}\right|^{cp}=\frac{1}{i\hbar}\sum_{\mathbf{q}}(\gamma_{\mathbf{q}}^{e}\langle d_{-\mathbf{k}}b_{\mathbf{q}}c_{\mathbf{k}-\mathbf{q}}\rangle+\gamma_{\mathbf{q}}^{e*}\langle d_{-\mathbf{k}}b_{\mathbf{q}}^{\dagger}c_{\mathbf{k}+\mathbf{q}}\rangle+\gamma_{\mathbf{q}}^{h}\langle b_{\mathbf{q}}d_{-\mathbf{k}-\mathbf{q}}^{\dagger}c_{\mathbf{k}}\rangle+\gamma_{\mathbf{q}}^{h*}\langle b_{\mathbf{q}}^{\dagger}d_{-\mathbf{k}+\mathbf{q}}c_{\mathbf{k}}\rangle). \tag{32}$$

Again, as in the case of carrier-carrier interaction, the first-order contributions are obtained by factorizing the expectation values on the right-hand side (rhs) of Eqs. (30)–(32). These expectation values, however, always contain a single-phonon creation or annihilation operator. If we neglect the possible existence of coherent phonon states, only operators corresponding to a well-defined phonon occupation number have nonvanishing expectation values. Thus, the first-order terms vanish. In order to obtain the second-order contribution, we first have to derive the equation of motion for the terms on the rhs of Eqs. (30)–(32). Neglecting the coupling to the light field (which would correspond to coupled phonon-photon processes and include the light-induced energy shifts), the result for the first term is given by

$$\frac{d}{dt}\langle c_{\mathbf{k}}^{\dagger}b_{\mathbf{q}}c_{\mathbf{k}-\mathbf{q}}\rangle=\frac{1}{i\hbar}(-\epsilon_{\mathbf{k}}^{e}+\epsilon_{\mathbf{k}-\mathbf{q}}^{e}+\hbar\omega_{\mathbf{q}})\langle c_{\mathbf{k}}^{\dagger}b_{\mathbf{q}}c_{\mathbf{k}-\mathbf{q}}\rangle+\frac{1}{i\hbar}\sum_{\mathbf{q}'}[\gamma_{\mathbf{q}}^{e}(\langle c_{\mathbf{k}}^{\dagger}b_{\mathbf{q}}b_{\mathbf{q}'}c_{\mathbf{k}-\mathbf{q}-\mathbf{q}'}\rangle-\langle c_{\mathbf{k}+\mathbf{q}'}^{\dagger}b_{\mathbf{q}'}b_{\mathbf{q}}c_{\mathbf{k}-\mathbf{q}}\rangle)+\gamma_{\mathbf{q}}^{e*}(\langle c_{\mathbf{k}}^{\dagger}b_{\mathbf{q}}b_{\mathbf{q}'}^{\dagger}c_{\mathbf{k}-\mathbf{q}+\mathbf{q}'}\rangle-\langle c_{\mathbf{k}-\mathbf{q}'}^{\dagger}b_{\mathbf{q}'}^{\dagger}b_{\mathbf{q}}c_{\mathbf{k}-\mathbf{q}}\rangle)]+\frac{1}{i\hbar}\sum_{\mathbf{k}'}(\gamma_{\mathbf{q}}^{e*}\langle c_{\mathbf{k}}^{\dagger}c_{\mathbf{k}'}^{\dagger}c_{\mathbf{k}'+\mathbf{q}}c_{\mathbf{k}-\mathbf{q}}\rangle+\gamma_{\mathbf{q}}^{h*}\langle c_{\mathbf{k}}^{\dagger}d_{\mathbf{k}'}^{\dagger}d_{\mathbf{k}'+\mathbf{q}}c_{\mathbf{k}-\mathbf{q}}\rangle) \tag{33}$$

and analogous equations for the other terms. They all have the form

$$\frac{d}{dt}x(t)=-i\omega x(t)+y(t), \tag{34}$$

where $y(t)$ contains expectation values of four operators. The second-order contribution is now obtained by factorizing $y(t)$ into distribution functions and polarizations. Then we have a closed set of equations of motion—not only for the distribution functions and polarizations, however, but also for expectation values of three operators. These can be eliminated by formally integrating Eq.

(34) according to

$$x(t)=x(t_0)e^{-i\omega(t-t_0)}+\int_0^{t-t_0}e^{-i\omega t'}y(t-t')dt' . \quad (35)$$

The result is a set of integro-differential equations for $f_{\mathbf{k}}^{e,h}$ and $p_{\mathbf{k}}$. The dynamics contains memory effects, and therefore it is non-Markovian.[47,51] This retardation can be eliminated by performing two additional approximations: the adiabatic and Markov approximations. The adiabatic approximation consists in adding a negative infinitesimal imaginary part η to ω and letting $t_0\rightarrow-\infty$. This means that the influence of any initial correlation has died out. For the Markov approximation we assume that $y(t)$ is slowly varying on the time scale relevant for the oscillation of the exponential function and thus can be taken in front of the integral. Performing the Markov approximation corresponds to a neglect of energy-nonconserving transitions involving phonons at short times.[51,59,60] The result of both approximations is

$$x(t)=\frac{1}{i\omega+\eta}y(t)=\left[-i\frac{\mathcal{P}}{\omega}+\pi\delta(\omega)\right]y(t) , \quad (36)$$

where $\mathcal{P}$ denotes the principal value. It should be noted that the polarizations by themselves are not slowly varying functions of time because even without external field, they are oscillating with a frequency given by the sum of electron and hole energy. This oscillation has to be taken into account in the exponential function, and only the remaining part can be taken as slowly varying.

The results finally obtained for carrier-phonon interaction within these approximations can be separated into two classes: the contributions corresponding to real scattering processes and those which are related to the presence of a polarization and vanish in the Boltzmann limit. The former ones involve interactions of a phonon with one type of carrier—the contributions contain the absolute square of the interaction matrix elements $|\gamma_{\mathbf{q}}^{e,h}|^2$—while the latter ones involve the simultaneous interactions with electrons and holes—they contain the product $\gamma_{\mathbf{q}}^{e}\gamma_{\mathbf{q}}^{h*}$ and its complex conjugate. In this work we will neglect this type of "polarization scattering"[59] and limit ourselves to scattering processes present in the Boltzmann limit.

The carrier-phonon contributions to the equations of motion for the distribution functions then turn out to be the standard Boltzmann scattering terms

$$\left.\frac{d}{dt}f_{\mathbf{k}}^{e,h}\right|^{cp}=\frac{2\pi}{\hbar}\sum_{\mathbf{q}}|\gamma_{\mathbf{q}}^{e,h}|^2\{\delta(\epsilon_{\mathbf{k}}^{e,h}-\epsilon_{\mathbf{k}-\mathbf{q}}^{e,h}-\hbar\omega)[N_{\mathbf{q}}f_{\mathbf{k}-\mathbf{q}}^{e,h}(1-f_{\mathbf{k}}^{e,h})-(N_{\mathbf{q}}+1)f_{\mathbf{k}}^{e,h}(1-f_{\mathbf{k}-\mathbf{q}}^{e,h})]$$
$$+\delta(\epsilon_{\mathbf{k}}^{e,h}-\epsilon_{\mathbf{k}+\mathbf{q}}^{e,h}+\hbar\omega_{\mathbf{q}})[(N_{\mathbf{q}}+1)f_{\mathbf{k}+\mathbf{q}}^{e,h}(1-f_{\mathbf{k}}^{e,h})-N_{\mathbf{q}}f_{\mathbf{k}}^{e,h}(1-f_{\mathbf{k}+\mathbf{q}}^{e,h})]\} . \quad (37)$$

The contribution to the polarization can be expressed in terms of the self-energy $\Sigma_{\mathbf{k}}^{cp}=\Sigma_{\mathbf{k}}^{e}+\Sigma_{\mathbf{k}}^{h}$ according to

$$\left.\frac{d}{dt}p_{\mathbf{k}}\right|^{cp}=\frac{1}{i\hbar}\Sigma_{\mathbf{k}}^{cp}p_{\mathbf{k}} , \quad (38)$$

in this case, however, with a complex self-energy. The real and imaginary parts [with $\Sigma_{\mathbf{k}}^{e,h}=\hbar(\Omega_{\mathbf{k}}^{e,h}-i\Gamma_{\mathbf{k}}^{e,h})$] are given by

$$\Omega_{\mathbf{k}}^{e,h}=\frac{1}{\hbar}\sum_{\mathbf{q}}|\gamma_{\mathbf{q}}^{e,h}|^2\left[\frac{\mathcal{P}}{\epsilon_{\mathbf{k}}^{e,h}-\epsilon_{\mathbf{k}-\mathbf{q}}^{e,h}-\hbar\omega_{\mathbf{q}}}[N_{\mathbf{q}}f_{\mathbf{k}-\mathbf{q}}^{e,h}+(N_{\mathbf{q}}+1)(1-f_{\mathbf{k}-\mathbf{q}}^{e,h})]\right.$$
$$\left.+\frac{\mathcal{P}}{\epsilon_{\mathbf{k}}^{e,h}-\epsilon_{\mathbf{k}+\mathbf{q}}^{e,h}+\hbar\omega_{\mathbf{q}}}[(N_{\mathbf{q}}+1)f_{\mathbf{k}+\mathbf{q}}^{e,h}+N_{\mathbf{q}}(1-f_{\mathbf{k}+\mathbf{q}}^{e,h})]\right] , \quad (39)$$

$$\Gamma_{\mathbf{k}}^{e,h}=\frac{\pi}{\hbar}\sum_{\mathbf{q}}|\gamma_{\mathbf{q}}^{e,h}|^2\{\delta(\epsilon_{\mathbf{k}}^{e,h}-\epsilon_{\mathbf{k}-\mathbf{q}}^{e,h}-\hbar\omega_{\mathbf{q}})[N_{\mathbf{q}}f_{\mathbf{k}-\mathbf{q}}^{e,h}+(N_{\mathbf{q}}+1)(1-f_{\mathbf{k}-\mathbf{q}}^{e,h})]$$
$$+\delta(\epsilon_{\mathbf{k}}^{e,h}-\epsilon_{\mathbf{k}+\mathbf{q}}^{e,h}+\hbar\omega_{\mathbf{q}})[(N_{\mathbf{q}}+1)f_{\mathbf{k}+\mathbf{q}}^{e,h}+N_{\mathbf{q}}(1-f_{\mathbf{k}+\mathbf{q}}^{e,h})]\} . \quad (40)$$

The real part of the self-energy has contributions depending on $f_{\mathbf{k}}^{e,h}$ as well as contributions independent of these quantities. When measuring the band structure of a material, the latter part is always present. It gives rise to the temperature dependence of the band gap and of the carrier effective mass. Thus, when specifying these quantities at a certain temperature, it is already included in H_0, and only the terms depending on $f_{\mathbf{k}}^{e,h}$ should be taken into account for calculating energy shifts.

By performing the same type of calculation, a Boltzmann equation for the distribution function of phonons $N_{\mathbf{q}}=\langle b_{\mathbf{q}}^{\dagger}b_{\mathbf{q}}\rangle$ can be obtained. The resulting complete set of equations allows one also to take into account hot-phonon effects.[11,19] In the present contribution, we will neglect this phenomenon and assume that the phonons always remain in equilibrium.

D. Carrier-photon interaction

The interaction with the coherent laser modes has already been taken into account in H_0. In addition, there is the interaction with the background photon field which

gives rise to the spontaneous emission and thus to the luminescence spectrum. Since the band gap is of the order of 1 eV, stimulated processes due to thermal photons are negligible at all relevant temperatures. The structure of the Hamiltonian is similar to that for carrier-phonon interaction; however, it connects electron and hole states. It is given in dipole and rotating-wave approximation by

$$H_1^{c\gamma}=\sum_{\mathbf{q},\mathbf{k},\nu}(\mu_{\mathbf{k}}c_{\mathbf{k}}^{\dagger}a_{\mathbf{q},\nu}d_{-\mathbf{k}}^{\dagger}+\mu_{\mathbf{k}}^{*}d_{-\mathbf{k}}a_{\mathbf{q},\nu}^{\dagger}c_{\mathbf{k}}) , \tag{41}$$

where $a_{\mathbf{q}'\nu}^{\dagger}$ ($a_{\mathbf{q},\nu}$) denote the creation (annihilation) operators of a photon with wave vector $\mathbf{q}$ and polarization index ν, and $\mu_{\mathbf{k}}$ represents the coupling matrix element which, except for a normalization constant, coincides with $M_{\mathbf{k}}$, introduced in Eq. (2). The contribution to H_0 is given by

$$H_0^{\gamma}=\sum_{\mathbf{q},\nu}\hbar\omega_q a_{\mathbf{q},\nu}^{\dagger}a_{\mathbf{q},\nu} , \tag{42}$$

with $\omega_q=cq$ and c being the light velocity.

Spontaneous recombination processes typically occur on much longer times than other scattering processes. Thus, for the ultrafast dynamics of the carrier system, they are of minor importance. However, in luminescence experiments the photon spectrum is the directly measured quantity. The recombination processes act as a detector of the state of the system and create the link between the theoretical calculation and the experimental output. Consequently, we will neglect the influence of carrier-photon interaction on the carrier dynamics and use this mechanism only to calculate the spectrum of the emitted photons.

The rate of emitted photons $R_{\mathbf{q},\nu}$ with wave vector $\mathbf{q}$ and polarization ν is given by

$$\begin{aligned}R_{\mathbf{q},\nu}&=\frac{d}{dt}\langle a_{\mathbf{q},\nu}^{\dagger}a_{\mathbf{q},\nu}\rangle\\&=\frac{1}{i\hbar}\sum_{\mathbf{k}}(-\mu_{\mathbf{k}}\langle c_{\mathbf{k}}^{\dagger}d_{-\mathbf{k}}^{\dagger}a_{\mathbf{q},\nu}\rangle+\mu_{\mathbf{k}}^{*}\langle a_{\mathbf{q},\nu}^{\dagger}d_{-\mathbf{k}}c_{\mathbf{k}}\rangle) .\end{aligned} \tag{43}$$

We now have to distinguish two cases: In the presence of an interband polarization there is coherent emission of photons. This is obtained by factorizing the products on the rhs of Eq. (43). We obtain

$$R_{\mathbf{q},\nu}^{\mathrm{coh}}=\frac{1}{i\hbar}\sum_{\mathbf{k}}(-\mu_{\mathbf{k}}p_{\mathbf{k}}^{*}\langle a_{\mathbf{q},\nu}\rangle+\mu_{\mathbf{k}}^{*}\langle a_{\mathbf{q},\nu}^{\dagger}\rangle p_{\mathbf{k}}) , \tag{44}$$

together with

$$\frac{d}{dt}\langle a_{\mathbf{q},\nu}\rangle=i\omega_{\mathbf{q}}\langle a_{\mathbf{q},\nu}\rangle+\frac{1}{i\hbar}\sum_{\mathbf{k}}\mu_{\mathbf{k}}^{*}p_{\mathbf{k}} . \tag{45}$$

If the polarization is created by the external field, the coherently emitted photons have the same direction as the incident field. Equations (44) and (45) are the basis for the analysis of four-wave-mixing and photon-echo experiments. When observing the luminescence in a direction different from that of the generating beam, this contribution vanishes. If the polarization is created by the internal field, the photons are emitted in all direction and Eqs. (44) and (45) describe exciton luminescence.

If there is no coherent interband polarization, this first-order contribution to the luminescence spectrum vanishes. Then, the right-hand side can be treated in analogy with carrier-phonon interaction, and the incoherent emission spectrum $I_{\mathrm{em}}^{0}(\omega_{\mathbf{q}})$ in second-order and Markov approximation is given by the golden-rule formula

$$I_{\mathrm{em}}^{0}(\omega_{\mathbf{q}})=R_{\mathbf{q},\nu}^{\mathrm{inc}}=\frac{2\pi}{\hbar}|\mu_{\mathbf{k}}|^2\delta(\epsilon_{\mathbf{k}}^{e}+\epsilon_{-\mathbf{k}}^{h}-\hbar\omega_{\mathbf{q}})f_{\mathbf{k}}^{e}f_{-\mathbf{k}}^{h} . \tag{46}$$

This is the emission spectrum of a free electron-hole gas. It does not contain renormalization and correlation effects which are of particular importance in regions close to the band gap. They can be included by taking into account in the equations of motion for the terms on the rhs of Eq. (43) the other types of interaction within the approximations discussed, i.e., carrier-carrier interaction in first order and carrier-phonon interaction in second order. We obtain for the first term in Eq. (43),

$$\begin{aligned}&\frac{d}{dt}\langle c_{\mathbf{k}}^{\dagger}d_{-\mathbf{k}}^{\dagger}a_{\mathbf{q},\nu}\rangle\\&\quad=\frac{1}{i\hbar}\sum_{\mathbf{k}'}\alpha_{\mathbf{k}\mathbf{k}'}(\omega_{\mathbf{q}})\langle c_{\mathbf{k}'}^{\dagger}d_{-\mathbf{k}'}^{\dagger}a_{\mathbf{q},\nu}\rangle-\mu_{\mathbf{k}}f_{\mathbf{k}}^{e}f_{-\mathbf{k}}^{h} ,\end{aligned} \tag{47}$$

with

$$\begin{aligned}\alpha_{\mathbf{k}\mathbf{k}'}(\omega)=&(\epsilon_{\mathbf{k}}^{e}+\epsilon_{-\mathbf{k}'}^{h}-\hbar\omega+\hbar\Omega_{\mathbf{k}}-i\hbar\Gamma_{\mathbf{k}})\delta_{\mathbf{k}\mathbf{k}'}\\&-(1-f_{\mathbf{k}}^{e}-f_{-\mathbf{k}}^{h})V_{\mathbf{k}-\mathbf{k}'}\end{aligned} \tag{48}$$

and the complex-conjugate equation for the second term. In this case, Eq. (47) cannot be simply integrated due to the nondiagonal character of the matrix $\alpha(\omega_{\mathbf{q}})$. However, in adiabatic and Markov approximation the spectrum is given by

$$\begin{aligned}I_{\mathrm{em}}(\omega_{\mathbf{q}})=&R_{\mathbf{q},\nu}^{\mathrm{inc}}\\&=\frac{1}{i\hbar}\sum_{\mathbf{k},\mathbf{k}'}\{\mu_{\mathbf{k}}\mu_{\mathbf{k}'}^{*}[\alpha^{-1}(\omega_{\mathbf{q}})]_{\mathbf{k}\mathbf{k}'}\\&\quad-\mu_{\mathbf{k}}^{*}\mu_{\mathbf{k}'}[\alpha^{*-1}(\omega_{\mathbf{q}})]_{\mathbf{k}\mathbf{k}'}\}f_{\mathbf{k}'}^{e}f_{-\mathbf{k}'}^{h} ,\end{aligned} \tag{49}$$

which requires for each frequency the inversion of the matrix $\alpha(\omega_{\mathbf{q}})$. This inversion can be performed numerically.[43,61]

Equation (49) connects the results of the carrier dynamics with the spectrum of emitted photons as observed in luminescence experiments. Another important experimental technique is given by excite and probe measurements. In this case, the absorption of a weak probe beam with amplitude A_p and frequency ω_p is analyzed. The light is absorbed due to the generation of carriers; thus the calculation of the absorption spectrum proceeds along the same lines as the calculation of the generation rate in Eqs. (8) and (23). Since the test beam is assumed to be weak, coherence effects associated with this light field do not play a role, and the adiabatic and Markov approximation can be applied. Neglecting the influence of the other types of interactions on the absorption process-

es, the spectrum is given by

$$I^0_{ab}(\omega_p)=\frac{1}{|A_p|^2}\sum_{\mathbf{k}} g^0_{\mathbf{k}}(\omega_p)$$
$$=\frac{2\hbar}{\hbar}\sum_{\mathbf{k}}|M_{\mathbf{k}}|^2\delta(\epsilon^e_{\mathbf{k}}+\epsilon^h_{-\mathbf{k}}-\hbar\omega_p)$$
$$\times(1-f^e_{\mathbf{k}}-f^h_{-\mathbf{k}}). \quad (50)$$

However, as in the case of the luminescence spectrum, at least close to the band gap the interaction effects cannot be neglected. They can be taken into account on the same level as in Eq. (47), leading to

$$I_{ab}(\omega_p)=\frac{1}{|A_p|^2}\sum_{\mathbf{k}} g_{\mathbf{k}}(\omega_p)$$
$$=\frac{1}{i\hbar}\sum_{\mathbf{k},\mathbf{k}'}\{\mathbf{M}_{\mathbf{k}}\mathbf{M}^*_{\mathbf{k}'}[\alpha^{-1}(\omega_{\mathrm{p}})]_{\mathbf{k}\mathbf{k}'}$$
$$-M^*_{\mathbf{k}}M_{\mathbf{k}'}[\alpha^{*-1}(\omega_p)]_{\mathbf{k}\mathbf{k}'}\}$$
$$\times(1-f^e_{\mathbf{k}'}-f^h_{-\mathbf{k}'}) . \quad (51)$$

The solution requires the inversion of the same matrix as for the case of emission. While the luminescence spectrum monitors the product of electron and hole distribution functions, the absorption spectrum gives information about their sum.

III. NUMERICAL METHOD

As discussed above, the aim of this paper is to extend the traditional Monte Carlo method for the solution of the Boltzmann equation[20,62,63] to the analysis of coherent phenomena, which are found to play a dominant role in the dynamic evolution of photoexcited semiconductors on short time scales. The main features which are not included in the traditional Monte Carlo method and that we want to take into account are the phase relations between different types of carriers (polarization phenomena), their interaction with an external coherent electromagnetic field (generation-recombination processes), and the correlation and renormalization effects associated with carrier-carrier interaction (Hartree-Fock terms). As shown in Sec. II, the task is therefore to solve numerically the system of equations of motion (9)–(11) for the distribution functions and the polarization, together with the generation rate, scattering terms, self-energies, and internal fields according to the interactions taken into account.

A. Semiclassical transport

In order to see the limitations of a "conventional" Monte Carlo simulation and to discuss the problems arising when trying to generalize it, let us briefly recall the basic ideas of the traditional approach to semiclassical transport.

The semiclassical limit in our case is obtained by eliminating the polarizations as independent variables. Since the internal field is directly related to the polarization, it has to be neglected. Excitonic effects cannot be described in this limit. The polarization is eliminated by solving Eq. (7) within the adiabatic and Markov approximations, as has been described for the case of carrier-phonon interaction. The result, however, does not include the broadening due to the energy-time uncertainty relation. It can be included by keeping the full time dependence of the light field and performing the Markov approximation only for the distribution functions and, if taken into account, the self-energies. For a Gaussian pulse

$$A_0(t)=A_L\exp\left[-\frac{(t-t_c)^2}{\tau_L^2}\right], \quad (52)$$

we obtain for the generation rate [Eq. (8)] in Markov approximation,

$$g_{\mathbf{k}}(t)=(2\pi)^{1/2}\left[\frac{M_k A_L}{\hbar}\right]^2\tau_L\exp\left[-2\frac{(t-t_c)^2}{\tau_L^2}\right]$$
$$\times\exp[-\tfrac{1}{2}(\tau_L\Delta\omega_{\mathbf{k}})^2][1-f^e_{\mathbf{k}}(t)-f^h_{-\mathbf{k}}(t)] , \quad (53)$$

where

$$\Delta\omega_{\mathbf{k}}=\omega_L-\frac{1}{\hbar}(\epsilon^e_{\mathbf{k}}+\epsilon^h_{-\mathbf{k}})-\Omega_{\mathbf{k}}$$

is the detuning of a transition from resonance. In the derivation it has been assumed that the imaginary part of the self-energy is much smaller than the inverse of the pulse width. In the opposite limit the result would be a Lorentzian broadening due to lifetime effects instead of the Gaussian broadening due to the finite pulse width.

With the Markovian generation rate (53), the Boltzmann equations (9) and (10) represent a set of rate equations. They are the basis for the traditional ensemble Monte Carlo (EMC) technique,[63] which simply provides a Monte Carlo solution of the above system of rate equations. Since all quantities which describe coherent properties are eliminated, this approach is obviously limited to the study of incoherent phenomena. Within the Monte Carlo method, an ensemble of N carriers is simulated (the total number N not necessarily being constant), each carrier i having its wave vector $\mathbf{k}_i$ (in space-dependent problems, its position vector $\mathbf{r}_i$ also). The solution of the equations can then be simply mapped onto a sequence of random "free flights," interrupted by random "scattering events."

For a linear Boltzmann equation, the scattering rates are fixed quantities and the individual carriers can evolve asynchronously. The situation becomes more complicated already in the semiclassical case, when the Boltzmann equations become nonlinear. This can have different origins: carrier-carrier scattering, the Pauli exclusion principle, hot phonons, or the presence of an electric field which has to be calculated self-consistently according to the Poisson equation. Now, the scattering rates or accelerating forces become time dependent via the time dependence of the distribution functions and the field. To treat these nonlinearities, a fixed time step has to be introduced, at the end of which the distribution functions are evaluated so that the new free flights and scattering rates can be determined.

Now let us look at the problems that we encounter when trying to treat coherent phenomena. First, of course, we have to solve also, in addition to the Boltzmann equations, the equation of motion for the polarization. Second, we have to deal with recombination processes due to the negative parts of the full generation rate (23). This is quite complicated within a "conventional" EMC. For the recombination process we need simultaneously an electron with wave vector $\mathbf{k}$ and a hole with wave vector $-\mathbf{k}$. Thus, in general, for each recombination process we have to check the states of all carriers to see if there is a pair with the desired wave vector (within a certain range in k space), and this pair can recombine. The origin of this problem is related to the fact that we have specified much more information than is necessary, and also, from a fundamental point of view, much more information than is possible. Implicitly, we have treated the carriers as distinguishable particles. However, the only relevant information would be to say, e.g., there is one carrier with $\mathbf{k}_1$, and not to say carrier 1 is in the state $\mathbf{k}_1$, etc., as is done in the simulation.

In what follows we propose a generalization of this traditional approach, which treats at the same time both coherent and incoherent phenomena. The generalized Monte Carlo method is derived starting directly from the original system of equations (9)–(11). The scope of the proposed approach is to combine the advantage of the stochastic simulation with the advantages of the direct technique for the solution of differential equations.

B. Numerical procedure for the quantum-kinetic model

The system of quantum-kinetic equations (9)–(11) is a system of nonlinear equations. The nonlinearities are present even in absence of carrier-carrier interaction due to the Pauli exclusion principle. The basic idea of the present approach is to perform a Monte Carlo simulation for the evaluation of the various distribution functions and a direct integration for the evaluation of the polarizations.

Due to the reasons discussed above, the usual representation of the carrier system is not appropriate for our problem. This "particle representation" (which corresponds to a classical picture) does not reflect the particle indistinguishability and, besides being redundant, introduces problems—in particular for the recombination processes. For these reasons we describe the state of the ensemble of carriers in the simulation by means of a "number representation" (which corresponds more directly to a "second-quantization" picture). It is obtained by introducing a phase-space discretization. For each cell characterized by a given wave vector $\mathbf{k}$ and a given band index ν, we specify the number $n_{\mathbf{k}}^{\nu}$ of carriers in the cell. This representation, if compared with the "particle representation," has the advantage of providing a clear and simple description of generation-recombination processes: Without checking all carriers, we immediately know if a recombination process with a given $\mathbf{k}$ is possible. This is due to the nature of this many-body approach which, by itself, strongly simplifies the treatment of physical systems characterized by a variable number of particles.

Besides the possibility of treating recombination processes in a simple way, this number representation has further advantages: From a fundamental point of view the indistinguishability is taken into account, and from a numerical point of view we can simulate a much larger number of carriers. In a particle representation, increasing the number of carriers means increasing the size of the vectors where the momentum is stored. In the number representation, the size of the vector is only determined by the number of cells and is independent of the number of carriers. Such a representation has recently been used in cellular-automata-type calculations for semiclassical transport in space-dependent problems.[53,54]

Given the set of "occupation numbers" $\{n_{\mathbf{k}}^{\nu}\}$ at time t, the distribution function $f_{\mathbf{k}}^{\nu}$ is obtained according to

$$f_{\mathbf{k}}^{\nu}=\frac{n_{\mathbf{k}}^{\nu}}{N_{\mathbf{k}}^{\nu}} \tag{54}$$

for each cell of the phase space, where $N_{\mathbf{k}}^{\nu}$ is the total number of available states in the cell. Thus, we can easily check the Pauli exclusion term $(1-f_{\mathbf{k}}^{\nu})$ in the scattering rates.

The basic lines of the simulation now proceed as follows: The total time is divided into time steps Δt. The simulation starts at the initial time $t=0$ before the laser has been switched on. The system is chosen to be in its fundamental state, that is, the vacuum of electron-hole pairs. This choice corresponds to initial distribution functions and polarizations equal to zero all over the phase space, and, therefore, the total number of simulated carriers is initially equal to zero.

The simulation then results in a loop over the sequence of time steps from the initial time up to the desired final time. At the beginning of each time step $t=t_i$, the system is completely specified by the distribution functions $f_{\mathbf{k}}^{\nu}$ and polarizations $p_{\mathbf{k}}$. From these quantities we calculate the self-energy $\Sigma_{\mathbf{k}}$, the field renormalization $\Delta_{\mathbf{k}}$, and the generation rate $g_{\mathbf{k}}$. Equation (11) for the polarization is then directly integrated from t_i to $t_i+\Delta t$. In this integration, the above-mentioned variables are approximated by their values at the beginning of the time step; the exponential functions occurring in the formal solution [which has the same structure as Eq. (35)], however, are integrated analytically.

The transport equations describing the distribution functions are solved by means of the standard Monte Carlo technique, that is, a stochastic estimate of the distribution function $f_{\mathbf{k}}^{\nu}$ at the time $t_i+\Delta t$ is performed using, as polarization and distribution functions for the nonlinear terms, the corresponding values at the initial time t_i. First, new electron-hole pairs are generated in the regions where $g_{\mathbf{k}}>0$, and electron-hole pairs are removed where $g_{\mathbf{k}}<0$. By integrating the rates, the total number of pairs to be generated and/or removed is calculated. Then, the wave vectors of the generated carriers are chosen at random according to the generation rate $g_{\mathbf{k}}$. In the number representation these processes are very simple; we just have to increase or decrease the number in the corresponding cell by 1.

Then, for each carrier an initial wave vector is determined at random with a constant probability distribution inside the cell. This is equivalent to the assumption of a constant distribution function in the cell and introduces no additional approximation than is already done when discretizing. A sequence of random free flights and random scattering events is generated in the standard way, until the carrier reaches the end of the time step. After each scattering event, in an intermediate counter the number in the initial cell is reduced by 1 and in the final one it is increased by 1. The choice of the scattering mechanism is first performed according to the rate without taking into account the Fermi factor $1-f_{\mathbf{k}}^{\nu}$. Then, a rejection technique is applied where the intermediate counter is taken for the determination of the actual occupation of the final state. Due to this method, the occupation number never exceeds the limit given by the number of states in a cell, as can happen if the distribution functions at the initial time are taken for the calculation of the Fermi factor.

For the case of isotropic systems, all the functions of $\mathbf{k}$ introduced before (i.e., occupation numbers, distribution functions, polarizations, total scattering rates, etc.) depend only on the absolute value of the wave vector k. Therefore, the phase-space discretization reduces to a discretization of k from $k=0$ up to a suitable $k=k_{\max}$. A cell at k_i is then given by the spherical shell in k space with

$$k_i-\tfrac{1}{2}\Delta k \le k < k_i+\tfrac{1}{2}\Delta k \ .$$

The total number of states in a cell N_k^{ν} increases quadratically with k_i. This may lead to small numbers of states in the cells with small k_i and thus to increasing fluctuations of the distribution functions in this region. Due to their small statistical weight, however, these fluctuations are irrelevant for observable quantities. These quantities always contain the density of states which decreases for small k values and therefore compensates the increase in the fluctuations. This holds also for the excitonic properties, e.g., in the absorption spectrum [Eq. (51)], as becomes obvious when converting the double sums over the three-dimensional vectors $\mathbf{k},\mathbf{k}'$ into integrals and performing the angular integrations.

IV. APPLICATIONS

In this section we present and discuss the results of several "simulated experiments" performed with the generalized Monte Carlo procedure described in Sec. III. Different physical conditions have been investigated: Section IV A is concerned with applications characterized by a central laser energy $\hbar\omega_L$ far from the band gap, while Sec. IV B describes some "simulated experiments" characterized by a laser energy close to or within the band gap.

For all these applications, a simplified GaAs semiconductor model has been employed: The band structure is given by a spherical and parabolic band for electrons and holes, respectively; carrier-carrier interaction has been introduced up to the first order in perturbation theory within the screened Hartree-Fock approximation; and, finally, carrier-phonon interaction is introduced within the Markov approximation for both polar optical and acoustic deformation-potential coupling. Terms that involve simultaneously interactions with electrons and holes ("polarization scattering"), however, have been neglected as discussed in Sec. II. In this first step we are mainly interested in the differences with respect to a "conventional" Monte Carlo simulation. Therefore, we have also neglected the real part of the self-energy due to electron-phonon interaction as given by Eq. (38) because the real part of the full self-energy is mainly determined by carrier-carrier interaction. The values of the semiconductor parameters used in the simulations are summarized in Table I.

The external laser field is introduced in terms of the vector potential $A(t)$ whose explicit form is given by Eq. (3) with a Gaussian pulse shape according to Eq. (52) for all simulations. For convenience, the amplitude A_L is given in terms of a Rabi frequency $\Omega_R=2M_{\mathbf{k}}A_L/\hbar$. The k dependence of the dipole matrix element has been neglected, and the central frequency ω_L is given in terms of an excess energy $E_{\text{exc}}=\hbar\omega_L-E_G$. The central time t_c of the laser pulse has been taken as twice the pulse width τ_L. The parameters chosen for the simulations are summarized in Table II. Here, the full GR model refers to a simulation where distribution functions and polarizations are calculated self-consistently according to Eq. (23), if Hartree-Fock terms are included, and to Eq. (8), if they are not included. The Markov model refers to a semiclassical simulation with the generation rate given by Eq. (53), where the polarization is not an independent variable. Thus, in the latter case no Hartree-Fock contributions can be included. The simulations can be divided

TABLE I. Material parameters used in the simulations. The parameters refer to a simplified GaAs model with two parabolic bands: the central valley of the conduction band and the heavy-hole band.

Band gap E_g	1.519 eV
Electron effective mass m_e	$0.063m_0$
Hole effective mass m_h	$0.450m_0$
Crystal density ρ	5.37 g/cm^3
Optical-phonon energy $\hbar\omega_{\text{op}}$	36.4 meV
Relative static dielectric constant ϵ_0	12.9
Relative optical dielectric constant ϵ_s	10.92
Longitudinal sound velocity s	5.33×10^5 cm/s
Acoustic deformation potential (electrons) E_e	5 eV
Acoustic deformation potential (holes) E_h	5 eV

TABLE II. Parameters chosen for the different simulations. Here, T_0 denotes the lattice temperature, E_{exc} the excess energy of the laser, τ_L the laser pulse width, Ω_R the Rabi frequency, and HF the inclusion of Hartree-Fock terms. The full GR model refers to Eqs. (8) and (23), the Markov model to Eq. (53).

Simulation number	T_0 (K)	E_{exc} (meV)	τ_L (ps)	Ω_R (10^{12} s^{-1})	HF	GR model
1	10	180	0.1	5	Yes	Full
2	10	180	0.1	5	No	Full
3	10	180	0.1	5	No	Markov
4	10	180	0.1	500	Yes	Full
5	10	−4.52	1	0.02	Yes	Full
6	10	−4.52	1	1	Yes	Full

into two classes: Excitations far from the gap, where energy relaxation and dephasing due to the coupling with phonons is important, and excitation close to or below the gap, where excitonic effects are important. It should be mentioned, however, that all the simulations are performed with the same program, varying only the input parameters and, of course, adjusting the time step to the physical relevant time scale.

A. Excitation far from gap

In this section we will examine the numerical results concerning simulations characterized by a laser energy far from the band gap. This is the typical situation for energy-relaxation experiments. First we want to investigate the case of a moderate final carrier density at low temperature such that the effects of degeneracy are not yet very important.

In Fig. 1 the self-consistent generation rates obtained from the Monte Carlo simulation are shown as a function

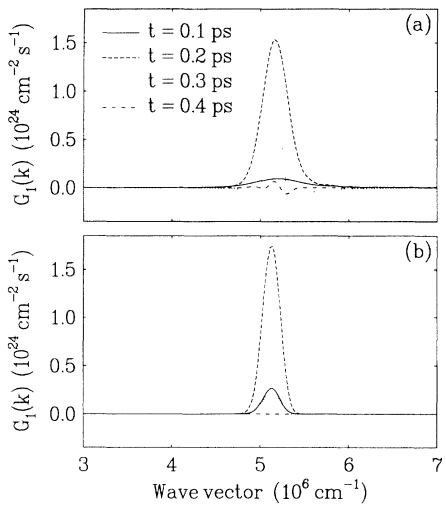

FIG. 1. Generation rate as a function of the wave vector k for different times: (a) taking into account the retardation and Hartree-Fock effects [Eq. (23)] and (b) in the Markovian limit without Hartree-Fock [Eq. (53)]. Case (a) shows the narrowing due to a recombination off resonance.

of the wave vector k for different times during the laser pulse. The plotted rate G_1 is obtained by integrating the generation rate over the angular variables:

$$G_1(k,t)=(2\pi)^{-3}\int g_k(t)k^2\sin\theta\, d\theta\, d\phi \tag{55}$$

and is proportional to the number of carriers generated in a spherical shell of the k space. Figure 1(a) shows the generation rates for the full generation model (simulation 1), while in Fig. 1(b) the corresponding rates for the Markovian model (simulation 3) are plotted. The latter ones are the rates used in a conventional Monte Carlo simulation. Due to the Markovian limit, they do not contain regions with negative values. On the contrary, the rates in Fig. 1(a) (which reflect the effects of the retardation in the generation-recombination process) also exhibit a strong time dependence in the shape. In particular, at short times (less than or of the order of the pulse width τ_L), the shape of the generation rate is found to be much broader than estimated from the uncertainty principle using the pulse width as uncertainty of time. The reason is that we have to use the "observation time" (i.e., the time since the start of the pulse) to estimate the linewidth. For longer times we note a narrowing of the generation rates; this narrowing, however, is accompanied by the buildup of negative regions off resonance which can be interpreted as a stimulated emission process. Thus, the distribution of the generated carriers not only becomes narrower with increasing time due to a generation mainly in resonance, but also due to a recombination of those carriers which have been generated performing energy-nonconserving transitions at short times. The final spreading in energy of the generated carriers then agrees with the value obtained from the uncertainty principle using the temporal spreading of the pulse.

These results show that a self-consistent treatment of the generation process can be important if either the evolution is already analyzed during the pulse or if some scattering mechanism is so strong that it can remove those carriers generated with the "wrong" energy before they can recombine. They also show that for this self-consistent model it is essential to treat recombination processes within the simulation.

In order to investigate the total effect of the recombination processes, we have plotted in Fig. 2(a) the integrated generation and recombination rates for the two simulations discussed above. We call a process genera-

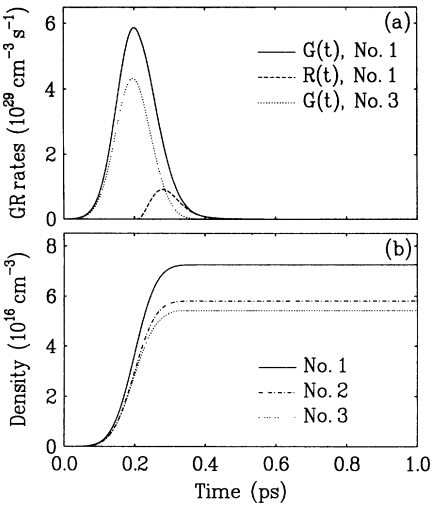

FIG. 2. (a) Total generation and recombination rate and (b) carrier concentration as functions of time for the Markovian limit and for the full generation model. The retardation and Hartree-Fock terms lead to a final density about 30% higher than in the Markovian limit. The effect is mainly due to Hartree-Fock terms, as can be seen from the dash-dotted line in (b), where the full GR model has been taken neglecting Hartree-Fock terms. The numbers refer to the simulation parameters in Table II.

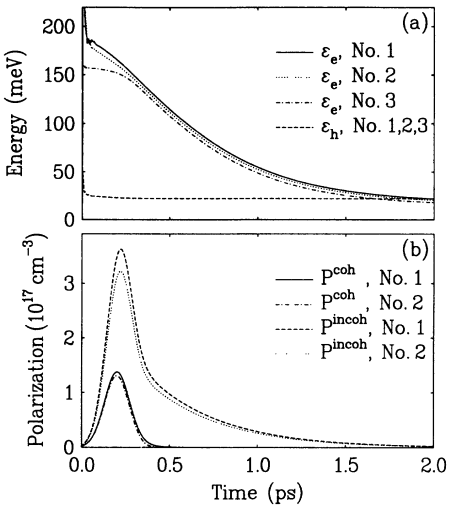

FIG. 3. (a) Kinetic energies of electrons and holes and (b) polarizations as functions of time for the retarded generation model with and without Hartree-Fock terms and for the Markovian model. In contrast to the density, here the full treatment of GR terms dominates over the Hartree-Fock effects. The energies of the holes do not exhibit significant differences in the various models. The energies of the electrons, however, are significantly larger at short times in the full model. The coherent polarization decays rapidly due to an inhomogeneous broadening in k space. The dephasing of the incoherently summed polarization is related to scattering processes, mainly with optical phonons.

tion if the rate at a given value of k is positive and recombination otherwise. Thus, the generation (recombination) rates are defined according to

$$G(t)=\int_0^\infty G_1(k,t)\Theta(G_1)dk \ , \tag{56}$$

$$R(t)=-\int_0^\infty G_1(k,t)\Theta(-G_1)dk \ , \tag{57}$$

where $\Theta(x)$ is the unit step function. We notice that the generation rate in the full model extends to substantially longer times due to retardation effects than in the Markovian limit. During the second half of the pulse, it is partially compensated by the recombination which reaches up to 15% of the maximum generation rate.

Figure 2(b) shows the carrier density as a function of time for simulations 1, 2, and 3. Comparing the dotted and dash-dotted curves, we find that the influence of the retardation in the generation process on the final density is not very important; the density is increased by less than 10%. Introducing Hartree-Fock, however, increases the density by about 30%. But this increase is relevant for the analysis of experiments only if the absolute laser intensity is known and if the light is absorbed only by the electronic system. Since this is not known quantitatively in many experiments, the laser intensity is calibrated with respect to the final carrier density generated, which means that we would have to take different laser intensities for the different models, and the experiments are not very sensitive to these differences.

In Fig. 3 the mean kinetic energies of electrons and holes (a) and the polarizations (b) are shown as functions of time for the different models. The energy of the holes is practically independent of the model, while the electron energy, in particular during the pulse, is increased in the retarded models. This can be understood from the energy uncertainty in the generation rate. The broadening at short times is symmetric in energy with respect to the laser frequency. The density of states, however, increases with increasing energy; thus it is more likely to generate carriers above resonance than below. In addition, of course, the stimulated emission then preferably removes these carriers [see Fig. 1(a), dotted line]. Therefore, after the end of the pulse, the difference is quite small. The Hartree-Fock terms lead to an additional slight increase in the electron energy. It can be partially attributed to the band-gap renormalization which shifts the position of the resonance to higher kinetic energies.

In Fig. 3(b) the solid and the dash-dotted curves refer to the absolute value of the total polarization, P^{coh}, defined as

$$P^{coh}=\left|\sum_{\mathbf{k}} p_{\mathbf{k}}\right| \ . \tag{58}$$

It decays due to the inhomogeneous broadening in k space since each contribution $p_{\mathbf{k}}$ in the sum rotates with a different frequency. The dotted and dashed curves refer to the incoherently summed polarization P^{incoh}, given by

$$P^{incoh}=\sum_{\mathbf{k}} |p_{\mathbf{k}}| \ . \tag{59}$$

It is a measure of the degree of coherence still present in the system, and it decays due to incoherent-scattering

processes. The relaxation times are of the order of 0.5 ps. In fact, this is the typical time related to the total scattering rate of the incoherent processes, which, at low temperatures, is mainly due to the optical-phonon emission. From an experimental point of view, the decay of the incoherently summed polarization can be directly measured by performing photon-echo experiments,[27] which, by performing a time reversal, tend to restore the initial coherent polarization according to the degree of coherence that has not yet been destroyed by scattering processes.

On the contrary, the coherent polarizations (solid and dash-dotted curves) decay with typical times that depend on the carrier distribution and, therefore, on the properties of the laser pulse. They reflect the coherent nature of both the carrier-carrier and the carrier-light interaction, and their time scale is typically much shorter than that related to incoherent phenomena.

Figure 4 shows the distribution functions of (a) electrons and (b) holes as a functions of the wave vector at different times obtained within the full model including Hartree-Fock terms. Since the holes are generated with a mean kinetic energy below the threshold for optical-phonon emission, the hole distribution practically remains constant after the end of the pulse. We notice a slight decrease of the maximum and an associated increase at the low-energy tail due to the interaction with acoustic phonons, which, however, is a much slower process than the interaction with optical phonons. On the contrary, the electron distribution shows the various replicas at multiples of the optical-phonon energy below the generation peak. At the latest time most of the carriers are already in the lowest replica. This explains why in Fig. 3(a) the electron energy has a nearly horizontal slope at the end. Relaxation due to emission of optical phonons has practically finished, and the subsequent relaxation due to emission of acoustic phonons is much slower.

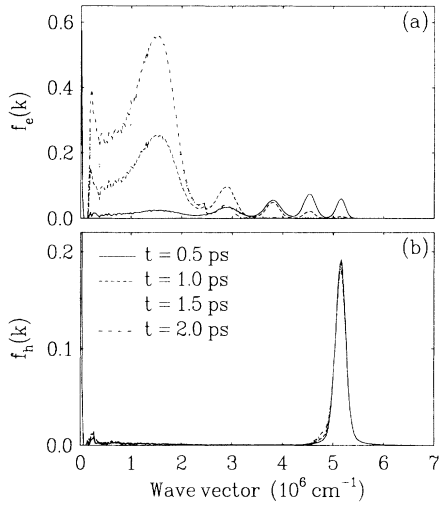

FIG. 4. Distribution functions of (a) electrons and (b) holes as functions of the carrier energy at different times. Since the holes are generated below the threshold for optical-phonon emission, the distribution practically remains constant after the end of the pulse. On the low-energy tail of the peak, the small relaxation due to emission of acoustic phonons is visible. The nonzero values at small wave vectors are associated with holes that have been generated at very short times above the threshold and then have emitted a phonon before performing a recombination. They are not significant due to their small statistical weight. The distribution of electrons shows the various replicas at multiples of the optical-phonon energy below the generation peak.

Figure 5 shows the generation rate as a function of the wave vector k at the end of the simulation. In the semiclassical limit there would be no generation or stimulated recombination of carriers after the end of the laser pulse. The internal field Δ_k due to electron-hole interaction, however, is still present and gives rise to generation-recombination processes according to Eq. (23). As discussed in Sec. II, this contribution does not affect the total number of generated electron-hole pairs (it vanishes when integrated with respect to k), but it acts on the corresponding carrier distribution in k space. We notice that the absolute value is much smaller than during the pulse [see Fig. 1(a)]; however, it is still detectable. The two distinct regions were G_1 has nonzero values are related to the regions in k space where the carriers are concentrated after the end of the relaxation process (see Fig. 4): The electrons have relaxed to low energies, and the holes are still in the region where they have been generated.

Now let us examine the self-energy. In Fig. 6(a) the real part (i.e., the band renormalization) is shown as a function of the wave vector at different times. With increasing time, due to the relaxation of the electrons, the region close to the band gap, in particular, shows a significant energy reduction. Figure 6(b) shows the imaginary part (divided by $\hbar$), the total incoherent-scattering rate. At time $t=0$ we have only the out-scattering contributions due to carrier-phonon interaction which is independent of the distribution functions. We see the two steps related to the threshold for optical-phonon emission of electrons and holes, and below the first step the much smaller scattering rate due to acoustic phonons. At later

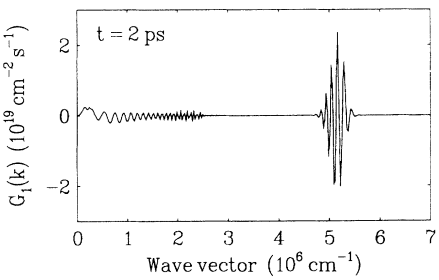

FIG. 5. Generation rate as a function of the wave vector for the simulation with Hartree-Fock terms as in Fig. 1(a). The effect of the internal field due to electron-hole interaction is not very large in this case far from gap; it is five orders of magnitude smaller than during the pulse [see Fig. 1(a)]; however, it is clearly visible in a generation rate which otherwise would be zero after the end of the light pulse.

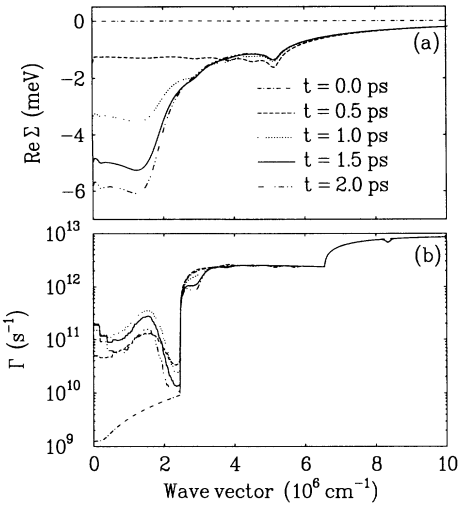

FIG. 6. (a) Real and (b) imaginary parts of the self-energy as functions of the wave vector at different times. The imaginary part is plotted in terms of the corresponding scattering rate Γ obtained according to Eq. (40). As explained in the text, for the real part only the contributions depending on the carrier distribution have been taken. Thus it is zero at time zero. When carriers are generated, initially this energy shift is concentrated around the generation region. At later times, due to the relaxation process, mainly the region close to the gap exhibits a lowering. The scattering rate at time zero contains only the out-scattering contributions. It shows the two steps related to the threshold for the emission of optical phonons by electrons and by holes and below the first threshold the small contribution of the acoustic phonons. At later times, the rate at small wave vectors is strongly increased due to in-scattering terms, while slightly above the first threshold, it is reduced due to phase-space filling.

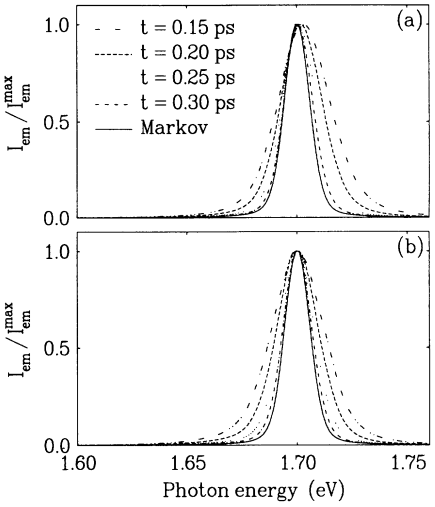

FIG. 7. Luminescence spectra (a) with and (b) without Hartree-Fock terms at different times during the presence of the laser pulse (the center of the pulse is at 0.2 ps). The spectra are normalized to their maxima in order to emphasize the changes in their shapes. Using the semiclassical Markov model, the shape does not depend on time and is given by the solid lines. Within the full GR model, the spectra reflect the time dependence of the broadening of the generation rate [Fig. 1(a)]. While this broadening is approximately symmetric without Hartree-Fock terms, their inclusion leads to a significant increase on the high-energy side of the spectrum.

times, the rates below the first threshold are strongly increased due to in-scattering contributions by emission of optical phonons. The region slightly above this threshold shows a significant reduction due to phase-space filling effects. The out-scattering process is reduced by the occupation of the final state which reaches values of about 0.6 [see Fig. 4(a)].

All the quantities discussed above help in understanding the physics of the carrier dynamics in a photoexcited semiconductor. However, they are not directly accessible by experiments. Therefore, in Fig. 7 the luminescence spectrum at different times is plotted as a function of the photon energy. Since we are far from the gap, the effect of electron-hole interaction for the spectrum is not very large, and we have neglected the off-diagonal terms in Eq. (48). The real and imaginary parts of the self-energy, however, have been taken into account. The calculated spectra refer to the luminescence not measured in the direction of the incident laser beam; thus only the incoherent part is shown.

We have shown the very early stage of the process, when the laser is still active, since at these times the differences between the models are most pronounced. Furthermore, all spectra are normalized with respect to their maxima in order to emphasize the line shape. In a semiclassical treatment, the generation rate is given by Eq. (53) and has a constant linewidth. Thus, the linewidth of the luminescence spectrum is also independent of time [solid lines in Figs. 7(a) and 7(b)]. Using the full generation model, on the other hand, we observe a strong time dependence of the luminescence line shape both with [Fig. 7(a)] and without [Fig. 7(b)] Hartree-Fock terms. During the pulse, the spectrum is remarkably broader, and it approaches the semiclassical result towards the end of the pulse. We do not see any effects of relaxation in the shape of the spectra because the holes practially do not relax. Thus, electrons that have emitted an optical phonon cannot contribute to the spectrum, which is sensitive only to the product of the distribution functions. Luminescence experiments are already performed in this very early stage, when the laser is still active;[7] therefore, coherent effects in the generation process should not be neglected in a theoretical analysis. In a real semiconductor the anisotropy, in particular, of the hole bands leads to an additional broadening in the carrier distributions.[25,64,65] This broadening, however, is independent of time and does not affect the discussion concerning the time-dependent broadening due to coherent effects.

All the above simulations have been performed in the regime where the effects of degeneracy are not yet very important (except in the low-energy part at the latest times, as discussed above). To check the method, we have performed a simulation where the laser amplitude has been increased by a factor of 100 so that we enter the

strongly degenerate regime (simulation 4 in Table II). In particular, the inverse of the Rabi frequency is now smaller than the pulse width and the typical relaxation times, which means that Rabi oscillations should be visible. Within the semiclassical generation rate [Eq. (53)], no strongly degenerate system can be generated. We can reach at most a half-filling of the bands. Then, the absorption changes into a stimulated emission process. Only a coherent light field can produce a complete inversion. We want to remark that this simulation is not intended to represent a realistic situation (in particular due to the absence of carrier-carrier scattering processes); rather, it demonstrates that the present approach, used for the solution of the set of kinetic equations, works under even these extreme conditions.

In Fig. 8 the generation-recombination rates (a) and the carrier density (b) are plotted as functions of time for this simulation. The rates now exhibit a strong modulation with recombination maxima between the generation maxima. This modulation leads to Rabi oscillations of the density. The oscillations do not return to zero as is the case in a two-level model in resonance, since in a semiconductor with a continuous energy spectrum, we always have off-resonance contributions.

The kinetic energies and polarizations as functions of time are plotted in Fig. 9. The Rabi oscillations during the presence of the pulse are visible in both quantities. The energy relaxation is reduced with respect to the nondegenerate case due to the occupation of the final states. In contrast to the nondegenerate case [Fig. 3(a)], the energy of the holes now exhibits an "overshoot" during the pulse.

Figure 10 shows the distribution functions of (a) electrons and (b) holes for this strongly degenerate case. When compared with the corresponding results of Fig. 4, here the distribution functions exhibit a generation broadening over a large energy range. Taking into account that the laser pulse duration is the same as in the previous simulations, it follows that this broadening is mainly a result of the phase-space filling, which cuts the generation rate in the regions of k space, where carriers already exist. The subsequent relaxation processes then lead to a practically complete filling of the low-energy states. The distribution functions tend towards Fermi-Dirac distributions. In the case of holes, however, the peak at the laser energy remains visible due to the fact

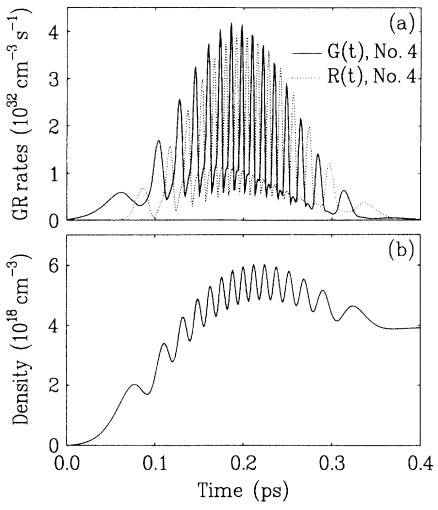

FIG. 8. (a) Generation and recombination rate and (b) carrier density for a strongly degenerate case. We observe strong Rabi oscillations in the density which are a purely coherent effect.

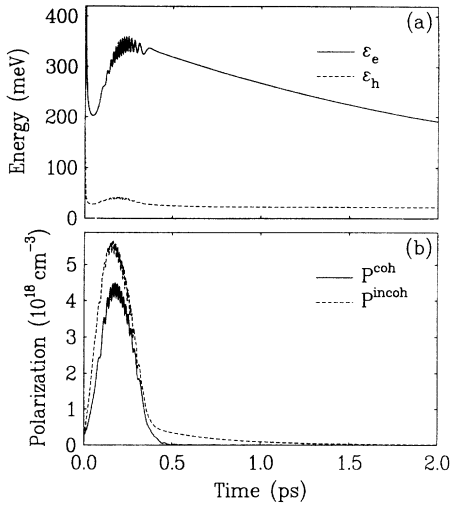

FIG. 9. (a) Kinetic energies of electrons and holes and (b) polarizations as functions of time for the strongly degenerate case. They also exhibit Rabi oscillations. The energy relaxation is reduced due to phase-space filling effects.

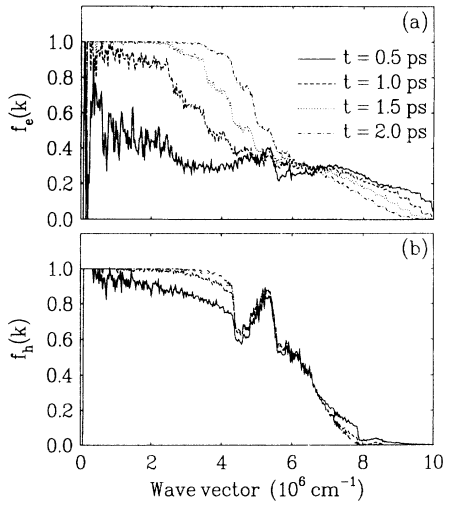

FIG. 10. Distribution functions of (a) electrons and (b) holes for the strongly degenerate case. The generation now is broadened over a large energy range. Taking into account that for the pulse duration the same value as for Fig. 5 has been taken, one can see that this broadening is mainly a result of the phase-space filling. The relaxation processes lead to a practically complete filling of the low-energy states.

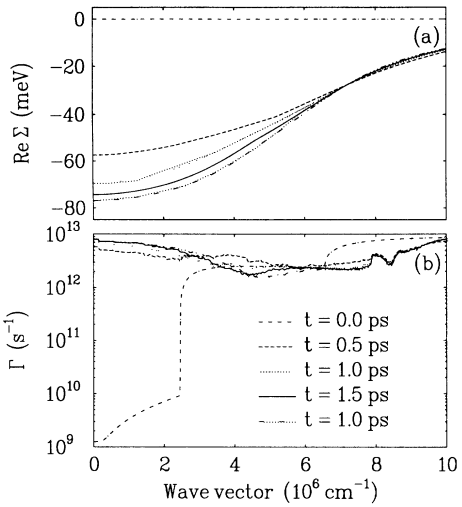

FIG. 11. (a) Real and (b) imaginary parts of the self-energy as functions of the wave vector at different times for the strongly degenerate case.

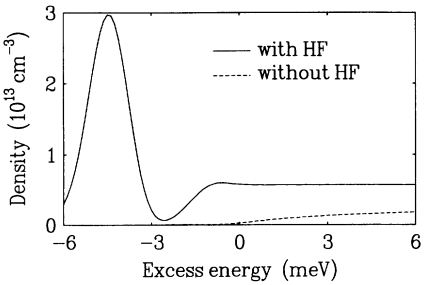

FIG. 12. Carrier density created by a laser pulse with fixed amplitude and a pulse width of 1 ps as a function of the excess energy of the laser. Except for the excess energy, all other parameters are unchanged and agree with simulation 5 (see Table II). As expected, without taking into account carrier-carrier interaction, the density is practically zero for excitation below the gap. Including Hartree-Fock terms, we recover the strong $n=1$ exciton line and a subsequent minimum between the $n=1$ and 2 exciton levels. The higher lines are not resolved due to the energy uncertainty associated with the short pulse duration.

that these carriers cannot emit an optical phonon. The distribution functions at low k values exhibit relatively strong fluctuations. This effect is a result of the small density of states in this region. Only one or a few carriers can occupy one cell leading to strong fluctuations, but the contributions to physical observables are statistically not significant (note that the total number of carriers in this simulation is of the order of 300 000 pairs).

Finally, in Fig. 11, the real and imaginary parts of the self-energy for this highly degenerate system are plotted. The band renormalization now reaches values as large as 80 meV at the end of the relaxation process, and the imaginary part does not show much structure. For all k values the total scattering rate after the end of the pulse is in the range of 10^{12} to 10^{13} s^{-1}.

B. Excitation close to gap

Let us now come to the analysis of the numerical results concerning laser excitations close to and within the band gap. This is the region where the effects due to Hartree-Fock terms are most pronounced and thus, besides giving insight in the physics, it serves as a check of the method. We have performed a series of simulations with different values of the excess energy, keeping constant all other simulation parameters. They are the same as for simulation 5 (see Table II).

Figure 12 shows the carrier density generated by a laser pulse with fixed amplitude and pulse width as a function of the excess energy. Both curves are obtained within the full generation model; for the solid curve the Hartree-Fock terms have been included, while the dashed curve refers to the simulation without Hartree-Fock terms. As expected, without taking into account carrier-carrier interaction, the density is practically zero for excitation below the gap. It starts slightly below the gap due to the finite pulse duration. Including Hartree-Fock terms, we recover the strong $n=1$ exciton line and a subsequent minimum between the $n=1$ and the $n=2$ exciton lines. The higher excited levels are not resolved due to the energy uncertainty associated with the short pulse duration.

In Fig. 13 the generation and recombination rates (a) and the carrier densities (b) are shown as functions of time for a laser excitation centered at the $n=1$ exciton level. The solid and dashed lines refer to a simulation with a weak laser field (simulation 5), while for the dotted and dash-dotted lines, the laser amplitude has been in-

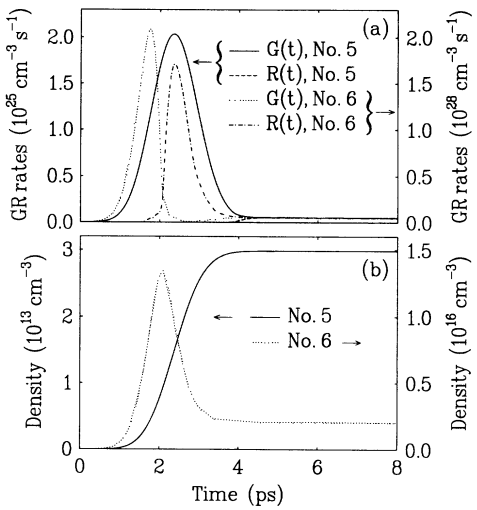

FIG. 13. (a) Generation and recombination rates and (b) carrier densities as functions of time for an excitation centered at the exciton ground state. Simulation 5 is performed with a weak laser field; the carrier density increases monotonically. In simulation 6 the laser amplitude has been increased by a factor of 50. In this case, during the second half of the pulse, there is a strong recombination, reducing the density to approximately 15% of its maximum value.

creased by a factor of 50 (simulation 6). For the weak excitation we observe a monotonic increase of the density. The inverse of the Rabi frequency is larger than the pulse duration and during the pulse there is practically no recombination. The maximum of the generation rate is slightly shifted in time with respect to the maximum of the laser pulse ($t_c = 2$ ps). This is a result of the retardation discussed in Sec. II. At the end of the pulse, the internal field due to electron-hole interaction leads to a recombination contribution that exactly cancels the generation rate. In the case of the strong excitation, on the other hand, the inverse of the Rabi frequency coincides with the pulse width. Thus, we enter the field of Rabi oscillations. In fact, close to the center of the pulse, the generation rate strongly decreases and about 85% of the carriers already generated recombine. Even if the laser power is increased by a factor of 2500, the final density is increased only by a factor of less than 100. After the end of the pulse, we again observe the role of the internal field leading to compensating generation and recombination rates.

Finally, let us return to the analysis of the spectrum. Figure 14 shows the absorption spectrum after the end of the laser pulse for simulations 5 and 6. The spectra have been calculated according to Eq. (51) using the numerical method described in Refs. 43 and 61. An additional lifetime broadening of 0.02 excitonic Ry has been included. In the case of weak excitation (solid line), we recover the equilibrium absorption spectrum, and the lowest three exciton lines are resolved. For high excitation the intensity of the ground-state absorption is slightly reduced; the effect, however, is quite weak since we are still below the Mott transition. As expected,[61] the position of the exciton ground state is unchanged. The first excited state is shifted by about 0.5 meV to lower energies as a result of the renormalization of the carrier energies as well as the renormalization of the interaction.

Figures 12 and 14 confirm the treatment of Hartree-Fock terms within our numerical simulation. From Fig. 12 it turns out that the calculation of the internal field according to Eq. (22) works very well. It reproduces a strong maximum in the density of generated carriers exactly at the expected energy of the exciton ground state. Figure 14 also confirms the calculation of the Hartree-Fock self-energy. The fact that the exciton ground state is not shifted when increasing the carrier density is a result of two compensating effects: The band gap is lowered due to the renormalization of the carrier energies, and the exciton binding energy is reduced due to a weakening of the interaction potential by the factor $(1-f^e_{\mathbf{k}}-f^h_{-\mathbf{k}})$, as can be seen most clearly in Eq. (48).

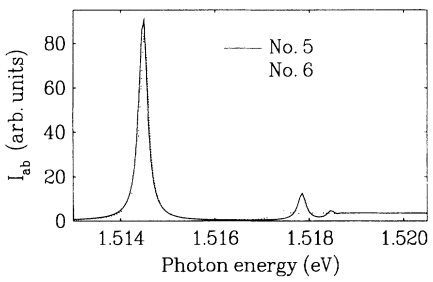

FIG. 14. Absorption spectra of the two simulations performed in resonance with the exciton ground state. In the case of a weak excitation, we recover the free spectrum, and the three lowest states are resolved. For high excitation the absorption at the ground state is slightly reduced, but the position is unchanged. The first excited state, however, exhibits a shift of about 0.5 meV.

V. CONCLUSIONS

We have presented a numerical method that enabled us to include coherent phenomena in a Monte Carlo simulation. The theory is based on the generalized optical Bloch equations for the distribution functions of electrons and holes, as well as for the interband polarization. The equation of motion for the polarization has been integrated directly, while the equations for the distribution functions have been solved by means of a Monte Carlo simulation. This method allowed us to simulate the generation process in a self-consistent way with its full time dependence. The generation rate contains retardation effects if compared with the standard Markov result used in semiclassical transport theory. With increasing time, this rate exhibits a narrowing in k space related to the energy-time uncertainty relation. In addition, it becomes partially negative, which can be interpreted as stimulated emission from the states off resonance and which contributes to the narrowing of the distribution of the generated carriers.

We have obtained the time dependence of the total polarization as well as of the incoherently summed polarization, which describes the degree of coherence still present in the system. Thus we can analyze the various times relevant for the dephasing process: the fast decay of the total polarization due to inhomogeneous broadening in k space and the decay of the incoherently summed polarization due to incoherent-scattering processes.

Since the light-matter interaction has been treated exactly, we were able to investigate the case of very intense pulses where we enter the strongly degenerate regime. An incoherent treatment of the generation process can never produce an inversion in the carrier system which is possible due to coherent effects. We have observed Rabi oscillations in the carrier density and related oscillations in other variables like carrier energy and polarizations. Since we have a continuum of states, the density never returns to zero, as would be the case for a coherently driven two-level atom in resonance.

The method further allowed us to introduce carrier-carrier interaction in Hartree-Fock approximation. Since this requires explicit knowledge of the polarization, it is not possible in a "conventional" Monte Carlo simulation. In general, the effects related to Hartree-Fock terms are not very important in regions far from the gap. However, due to the inclusion of these terms, we are also able to investigate phenomena close to the gap, where they strongly influence the dynamics as well as the luminescence and absorption spectra. We have found that the simulations recover the excitonic features well. We have

observed a strong resonance in the density of generated carriers when the laser is centered at the $n=1$ exciton line and a pronounced minimum between the $n=1$ and $n=2$ exciton. The higher excited states of the exciton were not resolved due to the linewidth of the laser pulse related to its finite pulse duration chosen in the simulations.

The presence of Rabi oscillations has also been found in the case of excitation at the exciton ground state. With increasing laser power, we observe the onset of stimulated recombination processes leading to a nonmonotonous temporal behavior of the carrier density. The treatment of Hartree-Fock terms within the simulations has been confirmed by the fact that exciton ground state is not shifted with increasing carrier density, in contrast to the excited states. The simulations with excitations close to the band gap have been performed without any changes in the program, which thus demonstrates that it allows us to investigate phenomena in the whole energy range.

Most results obtained in the present paper, however, cannot yet be compared directly with experiments. At least in the case of excitation far from gap and for not too small densities, carrier-carrier scattering processes play a dominant role in the dephasing process and also, even if they do not contribute directly, in the energy-relaxation process. They lead to a broad distribution of the carriers and therefore remove the strong threshold effects associated with the emission of optical phonons. Therefore, in a future work these scattering processes have to be taken into account. From the theoretical point of view, this means calculating the second-order contribution of carrier-carrier interaction within the adiabatic and Markov approximations.[47,49] For the numerical simulation these processes then have to be included in the Monte Carlo procedure for the distribution functions, as well as in the integration of the polarization. Furthermore, the existence of additional hole bands and valleys in the conduction band should be included, depending on the experiment to be described. Within the present approach, this does not represent a difficulty; we just have to use a distribution function for each band or valley, and a polarization for each pair of bands connected by the coherent light field. The present investigations, however, have shown that coherent phenomena in the theoretical analysis of ultrafast processes in semiconductors should not be neglected, even if only "incoherent" properties like carrier thermalization are studied.

ACKNOWLEDGMENTS

This work has been partially supported by the Consiglio Nazionale delle Ricerche (Rome, Italy) under the "Progetto Finalizzato MADESS." One of us (T.K.) acknowledges financial support from the Deutsche Forschungsgemeinschaft (Bonn, Germany).

*Permanent address: Institut für Theoretische Physik, Universität Stuttgart, Pfaffenwaldring 57, 7000 Stuttgart 80, Germany.

[1]J. Shah, Solid-State Electron. **32**, 1051 (1989).
[2]H. Kurz, Semicond. Sci. Technol. **7**, B124 (1992).
[3]J. F. Ryan and M. Tatham, Solid-State Electron. **32**, 1429 (1989).
[4]H. J. Polland, W. W. Rühle, H. J. Queisser, and K. Ploog, Phys. Rev. B **36**, 7722 (1987).
[5]K. Leo, W. W. Rühle, H. J. Queisser, and K. Ploog, Phys. Rev. B **37**, 7121 (1988).
[6]K. Leo, W. W. Rühle, H. J. Queisser, and K. Ploog, Appl. Phys. A **45**, 35 (1988).
[7]T. Elsaesser, J. Shah, L. Rota, and P. Lugli, Phys. Rev. Lett. **66**, 1757 (1991).
[8]R. G. Ulbrich, J. A. Kash, and J. C. Tsang, Phys. Rev. Lett. **62**, 949 (1989).
[9]J. A. Kash, in *The Physics of Semiconductors,* edited by E. M. Anastassakis and J. D. Joannopoulos (World Scientific, Singapore, 1990), p. 2459, and Phys. Rev. B **40**, 3455 (1989).
[10]C. W. W. Bradley, R. A. Taylor, and J. F. Ryan, Solid-State Electron. **32**, 1173 (1989).
[11]W. Pötz and P. Kocevar, Phys. Rev. B **28**, 7040 (1983).
[12]K. Leo and J. H. Collet, Phys. Rev. B **44**, 5535 (1991).
[13]T. F. Zhang, W. Cai, P. Hu, and M. Lax, Solid-State Electron. **32**, 1089 (1989).
[14]J. Collet and T. Amand, Physica B **134**, 394 (1985).
[15]J. Collet and T. Amand, J. Phys. Chem. Solids **47**, 153 (1986).
[16]R. Binder, D. Scott, A. E. Paul, M. Lindberg, K. Henneberger, and S. W. Koch, Phys. Rev. B **45**, 1107 (1992).
[17]A. A. Grinberg and S. Luryi, Phys. Rev. Lett. **65**, 1251 (1990).
[18]M. A. Osman and D. K. Ferry, Phys. Rev. B **36**, 6018 (1987).
[19]P. Lugli, P. Bordone, L. Reggiani, M. Rieger, P. Kocevar, and S. M. Goodnick, Phys. Rev. B **39**, 7852 (1989).
[20]P. Lugli, P. Bordone, S. Gualdi, L. Rota, and S. M. Goodnick, in *NASECODE VI,* Proceedings of the Sixth International Conference on the Numerical Analysis of Semiconductor Devices and Integrated Circuits, edited by J. J. H. Miller (Boole, Dublin, 1989), p. 238.
[21]L. Rota, P. Poli, C. Jacoboni, and P. Lugli, in *The Physics of Semiconductors,* edited by E. M. Anastassakis and J. D. Joannopoulos (World Scientific, Singapore, 1990), p. 2534.
[22]M. J. Kann, A. M. Kriman, and D. K. Ferry, Proc. Soc. Photo-Opt. Instrum. Eng. **1282**, 98 (1990).
[23]C. J. Stanton, D. W. Bailey, and K. Hess, IEEE J. Quantum Electron. **QE-24**, 1614 (1988).
[24]C. J. Stanton, D. W. Bailey, and K. Hess, Phys. Rev. Lett. **65**, 231 (1990).
[25]D. W. Bailey, C. J. Stanton, and K. Hess, Phys. Rev. B **42**, 3423 (1990).
[26]D. K. Ferry, A. M. Kriman, H. Hida, and S. Yamaguchi, Phys. Rev. Lett. **67**, 633 (1991).
[27]P. C. Becker, H. L. Fragnito, C. H. Brito Cruz, R. L. Fork, J. E. Cunningham, J. E. Henry, and C. V. Shank, Phys. Rev. Lett. **61**, 1647 (1988).
[28]A. Honold, L. Schultheis, J. Kuhl, and C. W. Tu, Appl. Phys. Lett. **52**, 2105 (1988).
[29]E. O. Göbel, Adv. Solid State Phys. **30**, 269 (1990).
[30]K. Leo, M. Wegener, J. Shah, D. S. Chemla, E. O. Göbel, T. C. Damen, S. Schmitt-Rink, and W. Schäfer, Phys. Rev. Lett. **65**, 1340 (1990).
[31]K. Leo, T. C. Damen, J. Shah, E. O. Göbel, and K. Köhler, Appl. Phys. Lett. **57**, 19 (1990).
[32]E. O. Göbel, K. Leo, T. C. Damen, J. Shah, S. Schmitt-Rink,

W. Schäfer, J. F. Müller, and K. Köhler, Phys. Rev. Lett. **64**, 1801 (1990).
[33]G. Noll, U. Siegner, S. G. Shevel, and E. O. Göbel, Phys. Rev. Lett. **64**, 792 (1990).
[34]V. Langer, H. Stolz, and W. von der Osten, Phys. Rev. Lett. **64**, 854 (1990).
[35]K. Leo, E. O. Göbel, T. C. Damen, J. Shah, S. Schmitt-Rink, W. Schäfer, J. F. Müller, K. Köhler, and P. Ganser, Phys. Rev. B **44**, 5726 (1991).
[36]W. H. Knox, D. S. Chemla, D. A. B. Miller, J. B. Stark, and S. Schmitt-Rink, Phys. Rev. Lett. **62**, 1189 (1989).
[37]A. Mysyrowicz, D. Hulin, A. Antonetti, A. Migus, W. T. Masselink, and H. Markoc, Phys. Rev. Lett. **56**, 2748 (1986).
[38]C. Comte and G. Mahler, Phys. Rev. B **34**, 7164 (1986).
[39]C. Comte and G. Mahler, Phys. Rev. B **38**, 10 517 (1988).
[40]A. Stahl, Z. Phys. B **72**, 371 (1988).
[41]A. Stahl, Phys. Status Solidi B **150**, 327 (1988).
[42]I. Balslev, R. Zimmermann, and A. Stahl, Phys. Rev. B **40**, 4095 (1989).
[43]H. Haug, in *Optical Nonlinearities and Instabilities in Semiconductors,* edited by H. Haug (Academic, San Diego, 1988), p. 53.
[44]S. Schmitt-Rink, C. Ell, and H. Haug, Phys. Rev. B **33**, 1183 (1986).
[45]S. Schmitt-Rink, D. S. Chemla, and H. Haug, Phys. Rev. B **37**, 941 (1988).
[46]R. Zimmermann, Phys. Status Solidi B **146**, 545 (1988).
[47]A. V. Kuznetsov, Phys. Rev. B **44**, 8721 (1991).
[48]S. Schmitt-Rink and D. S. Chemla, Phys. Rev. Lett. **57**, 2752 (1986).
[49]M. Lindberg and S. W. Koch, Phys. Rev. B **38**, 3342 (1988).
[50]M. Lindberg and S. W. Koch, Phys. Status Solidi B **150**, 379 (1988).
[51]R. Zimmermann, Phys. Status Solidi B **159**, 317 (1990).
[52]R. Zimmermann and M. Hartmann, Phys. Status Solidi B **150**, 365 (1988).
[53]M. Rieger and P. Vogl, Solid-State Electron. **32**, 1399 (1989).
[54]K. Kometer, G. Zandler, and P. Vogl, Semicond. Sci. Technol. **7**, B559 (1992).
[55]L. P. Kadanoff and G. Baym, *Quantum Statistical Mechanics* (Benjamin, New York, 1962).
[56]E. M. Lifshitz and L. P. Pitaevskii, *Physical Kinetics* (Pergamon, Oxford, 1981).
[57]C. Klingshirn, in *Optical Nonlinearities and Instabilities in Semiconductors,* edited by H. Haug (Academic, San Diego, 1988), p. 13, and other contributions in this volume.
[58]F. Bechstedt and S. Glutsch, J. Phys. Condens. Matter **3**, 7145 (1991).
[59]A. V. Kuznetsov, Phys. Rev. B **44**, 13 381 (1991).
[60]R. Brunetti, C. Jacoboni, and F. Rossi, Phys. Rev. B **39**, 10 781 (1989).
[61]S. Schmitt-Rink, J. Löwenau, and H. Haug, Z. Phys. B **47**, 13 (1982).
[62]C. Jacoboni and L. Reggiani, Rev. Mod. Phys. **55**, 645 (1983).
[63]C. Jacoboni and P. Lugli, in *The Monte Carlo Method for Semiconductor Device Simulation* (Springer, Wien, 1989).
[64]G. Fasol and H. P. Hughes, Phys. Rev. B **33**, 2953 (1986).
[65]G. Fasol, W. Hackenberg, H. P. Hughes, K. Ploog, E. Bauser, and H. Kano, Phys. Rev. B **41**, 1461 (1990).